Loop and Subdomain Movements in the Mechanism of *Escherichia coli* Dihydrofolate Reductase: Crystallographic Evidence[†,‡]

Michael R. Sawaya* and Joseph Kraut

Department of Chemistry and Biochemistry, University of California, San Diego, 9500 Gilman Drive, La Jolla, California 92093-0506

Received September 16, 1996; Revised Manuscript Received November 18, 1996[⊗]

ABSTRACT: The reaction catalyzed by *Escherichia coli* dihydrofolate reductase (ecDHFR) cycles through five detectable kinetic intermediates: holoenzyme, Michaelis complex, ternary product complex, tetrahydrofolate (THF) binary complex, and THF·NADPH complex. Isomorphous crystal structures analogous to these five intermediates and to the transition state (as represented by the methotrexate·-NADPH complex) have been used to assemble a 2.1 Å resolution movie depicting loop and subdomain movements during the catalytic cycle (see Supporting Information). The structures suggest that the M20 loop is predominantly closed over the reactants in the holoenzyme, Michaelis, and transition state complexes. But, during the remainder of the cycle, when nicotinamide is not bound, the loop occludes (protrudes into) the nicotinamide−ribose binding pocket. Upon changing from the closed to the occluded conformation, the central portion of the loop rearranges from β-sheet to 3_{10} helix. The change may occur by way of an irregularly structured open loop conformation, which could transiently admit a water molecule into position to protonate N5 of dihydrofolate. From the Michaelis to the transition state analogue complex, rotation between two halves of ecDHFR, the adenosine binding subdomain and loop subdomain, closes the (*p*-aminobenzoyl)glutamate (pABG) binding crevice by ≈0.5 Å. Resulting enhancement of contacts with the pABG moiety may stabilize puckering at C6 of the pteridine ring in the transition state. The subdomain rotation is further adjusted by cofactor-induced movements (≈0.5 Å) of helices B and C, producing a larger pABG cleft in the THF·NADPH analogue complex than in the THF analogue complex. Such movements may explain how THF release is assisted by NADPH binding. Subdomain rotation is not observed in vertebrate DHFR structures, but an analogous loop movement (residues 59−70) appears to similarly adjust the pABG cleft width, suggesting that these movements are important for catalysis. Loop movement, also unobserved in vertebrate DHFR structures, may preferentially weaken $NADP^+$ *vs* NADPH binding in ecDHFR, an evolutionary adaptation to reduce product inhibition in the $NADP^+$ rich environment of prokaryotes.

Dihydrofolate reductase (DHFR,[1] EC 1.5.1.3) is a biologically universal housekeeping enzyme which catalyzes the NADPH-linked reduction of 7,8-dihydrofolate to 5,6,7,8-tetrahydrofolate. Its clinical importance is derived from the fact that it is principally responsible for maintaining intracellular pools of THF. THF, in turn, is the cofactor used in synthesis of several other important metabolites (Blakley, 1969), one of which is thymidylate, a building block of DNA. Hence, DHFR has long been recognized as a drug target for inhibiting DNA synthesis in rapidly proliferating cells such as cancer cells (Huennekens, 1994) or bacterial or malarial infections (Roth & Stammers, 1992).

The importance of its clinical role has made DHFR a long-standing target of enzymological studies. Since the 1950s, researchers have been working toward a detailed picture of how the enzyme works by studying its kinetics and structure (Huennekens, 1996). Major advances include elucidation of a full kinetic pathway for DHFRs of *Escherichia coli* (Fierke et al., 1987), *Pneumocystis carinii* (Margosiak et al., 1993), mouse (Thillet et al., 1990), and human (Appleman et al., 1990). Crystallographic and NMR studies have elucidated the structure of DHFRs from *Lactobacillus casei* (Matthews et al., 1978; Bolin et al., 1982; Filman et al., 1982; Morgan et al., 1995), chicken (Matthews et al., 1985a,b; Volz et al., 1982; McTigue et al., 1992, 1993), human (Oefner et al., 1988; Davies et al., 1990; Cody et al., 1993), mouse (Stammers et al., 1987), *P. carinii* (Champness et al., 1994), and *Leishmania major* (Knighton et al., 1994). But the most extensive structural characterization has been done for *E. coli* DHFR (Table 1).

Still unknown is the enzyme's conformational behavior as a function of progress along the reaction coordinate. The reaction catalyzed by ecDHFR has been shown to cycle through five intermediate states under cellular conditions of substrate and cofactor concentration: holoenzyme, Michaelis complex, ternary product complex, THF binary complex, and THF·NADPH complex (Fierke et al., 1987). But we do not

[†] Supported by NIH Grant CA17374 and Training Grants DK07233 and HG00005 from the Public Health Service.

[‡] Coordinates and reflection data are available from the Brookhaven Protein Data Bank. See Table 1 for PDB entry codes.

* To whom correspondence should be addressed.

[⊗] Abstract published in *Advance ACS Abstracts,* January 1, 1997.

[1] Abbreviations: ATP-ribose, 2′-monophosphoadenosine 5′-diphosphoribose; ddTHF, 5,10-dideazatetrahydrofolate; DHF, 7,8-dihydrofolate; DHFR, dihydrofolate reductase; ecDHFR, dihydrofolate reductase from *Escherichia coli*; FOL, folate; KHP, potassium hydrogen phthalate; MTX, methotrexate; NADP, either $NADP^+$ or NADPH; $NADP^+$ and NADPH, nicotinamide adenine dinucleotide phosphate (oxidized and reduced, respectively); pABA, *p*-aminobenzoic acid; pABG, (*p*-aminobenzoyl)glutamate; PEG, polyethylene glycol; RMS, root mean square; THF, (6*S*)-5,6,7,8-tetrahydrofolate.

S0006-2960(96)02337-9 CCC: $14.00

Table 1: *E. coli* DHFR Crystal Structures

complex	space group[a]	cell dimensions				crystallization medium				data	*R* factor	PDB	
		a (Å)	*b* (Å)	*c* (Å)	*β* (deg)	ethanol (%)	Ca^{2+} (mM)	PEG (%)	pH	(Å)	(%)	code	footnote
$NADP^+$	*C*2	75.0	59.4	38.9	106		11	30	7.0	1.5	16.9	1ra9	*c*
NADPH		74.9	59.2	38.9			11	30	7.0	1.9	14.7	1ra1	*c*
thio-$NADP^+$		74.9	59.5	39.0			11	28	7.0	1.9	18.1		*d*
dihydrobiopterin·$NADP^+$		74.9	59.3	39.0			11	35	7.0	1.8	15.4		*d*
FOL·ATP-ribose		74.2	59.9	39.0			10	32	7.0	1.8	14.4	1ra8	*c*
FOL·$NADP^+$		74.2	59.9	39.0			10	32	7.0	1.6	17.1	1ra2	*c*
MTX·$NADP^+$		74.9	60.2	38.9			11	30	6.0	1.8	17.0	1ra3	*c*
FOL·$NADP^+$	$P2_1$[b]	41.8	75.7	59.1	99		90	25	8.0	2.1	20.5	1rb2	*c*
MTX·$NADP^+$		41.6	74.2	59.2			50	25	7.0	2.3	16.0	1rb3	*c*
$NADP^+$	$P2_12_12_1$[A]	34.8	59.0	81.3			100	9	7.0	2.4	19.8	6dfr	*e*
ddTHF·$NADP^+$		34.8	59.1	81.0			50	25	7.2	1.9	17.9	1rc4	*c*
ddTHF	$P2_12_12_1$[B]	34.8	44.8	100.8			300 (Mn^{2+})	16	7.4	2.3	17.4	1rx5	*c*
DHF		34.8	44.6	100.8			300 (Mn^{2+})	13	5.3	1.9	20.9		*f*
FOL		35.0	45.3	101.1			300 (Mn^{2+})	20	6.5	2.3	18.1	1rx7	*c*
$NADP^+$		34.4	45.5	99.2			300	15	7.0	1.9	18.4	1rx9	*c*
NADPH		34.5	45.4	98.7			450	25	8.0	2.0	18.0	1rx1	*c*
ddTHF·ATP-ribose		34.9	45.1	100.9			300	20	6.0	2.2	17.5	1rx4	*c*
ddTHF·NADPH		34.9	45.3	101.1			300	20	7.0	2.0	18.4	1rx6	*c*
DHF·$NADP^+$		34.3	45.6	98.9			300 (Mn^{2+})	14	5.3	1.8	17.9		*f*
FOL·ATP-ribose		34.4	45.0	99.3			300 (Mn^{2+})	16	7.0	2.8	14.4	1rx8	*c*
FOL·$NADP^+$		34.3	45.5	98.9			300 (Mn^{2+})	16	7.0	1.8	17.1	1rx2	*c*
MTX·NADPH		34.4	45.5	98.7			300 (Mn^{2+})	23	7.0	2.2	15.6	1rx3	*c*
FOL	$P2_12_12_1$[C] [b]	49.2	65.7	116.9			100 (Na^+)	30	8.5	2.6	16.3	1rd7	*c*
FOL	$P2_12_12_1$[D] [b]	44.4	60.9	122.0			200 (Mg^{2+})	26	8.0	2.6	17.8	1re7	*c*
DHF	$P2_12_12_1$[E]	34.7	38.9	108.8			210	16	6.6	1.8	17.0	1rf7	*c*
MTX	$P2_12_12_1$[F]	37.0	62.6	65.6			50	25	7.2	2.0	17.0	1rg7	*c*
Apo	$P3_121$	68.7	68.7	83.5				25	5.4	2.3	19.2	5dfr	*g*
NADPH	$P3_221$	62.0	62.0	107.7		2	8	25	7.0	2.3	20.1	1drh	*c*
FOL·$NADP^+$		62.2	62.2	105.5		3	11	12	6.0	2.5	24.5	7dfr	*e*
MTX·$NADP^+$		63.0	63.0	105.8		3	10	12	6.0	2.6	21.6	1dre	*c*
MTX·NADPH		62.5	62.5	105.8			8	29	7.0	2.4	22.8	1rh3	*c*
TMP·NADPH		61.8	61.8	105.8		2	4		6.8	3.0	44		*h*
5-deazafolate	$P6_1$[b]	93.1	93.1	73.9		21	50		6.8	2.0	14.9	1dyh	*i*
6-methylpterin		93.1	93.1	73.9		21	50		6.8	1.9	15.7		*j*
6-methylpterin·pABA		93.2	93.2	74.2		21	50		6.8	2.1	16.2		*j*
6-methylpterin·pABG		93.0	93.0	73.6		21	50		6.8	1.9	15.7		*j*
biopterin		93.1	93.1	73.9		21	50		6.8	1.9	14.7		*j*
ddTHF		93.1	93.1	73.9		21	50		6.8	2.0	14.5	1dyj	*i*
dihyrobiopterin		93.0	93.0	73.4		21	50		6.8	2.0	14.0		*d*
DHF		93.0	93.0	73.7		18	50		7.0	2.0	14.0		*f*
FOL		93.1	93.1	73.8		21	50		6.8	2.0	13.7	1dy1	*i*
folinic acid		92.6	92.6	73.1		21	50		6.8	2.0	14.2	1jol	*k*
MTX		93.1	93.1	73.9		21	5		6.8	1.7	15.5	3drc	*l*
pABA		92.1	92.1	73.4		21	50		6.8	2.0	15.8		*j*
pABG		93.2	93.2	73.8		21	50		6.8	2.0	16.2		*j*
TMP		93.1	93.1	73.9		21	5		6.8	1.7	15.5		*m*
folinic acid	$P6_5$	96.9	96.9	35.0		22	5		6.8	2.0	14.2	1jom	*k*

[a] Capital letter superscripts are used to distinguish between different lattices of $P2_12_12_1$. [b] Two molecules per asymmetric unit. [c] This work. [d] Crystals characterized by H. Lee. [e] Bystroff et al. (1990). [f] Crystals characterized by Y. Chen. [g] Bystroff and Kraut (1991). [h] Champness et al. (1986). [i] Reyes et al. (1995). [j] Crystals characterized by V. Reyes. [k] Lee et al. (1996). [l] Matthews et al. (1977), Bolin et al. (1982), and Filman et al. (1982). [m] Matthews et al. (1985a).

yet have a dynamical picture of how the enzyme may alter its conformation as it binds to these intermediates. If such a movie of molecular conformational motions were available, it would help complete our picture of how catalysis is achieved, from the initial binding of substrates to the release of products. Understanding the role of conformational motions may also shed light on how mutations far from the active site manifest their effects on kinetic parameters (Adams et al., 1989; Li et al., 1991; Dion et al., 1993; Howell et al., 1990).

Previous structural studies have already revealed some aspects of ecDHFR's conformational flexibility. Among the most prominent displays of flexibility are loop movements and subdomain rotation. NMR studies of the apoenzyme indicate that the M20 loop, the active site loop of ecDHFR, oscillates at a frequency similar to k_{cat} (Falzone et al., 1994). Crystallographic snapshots of various ligand complexes revealed that these loop movements involve displacements of up to 5 Å and that relative rotation between DHFR's two subdomains produces differences in pABG cleft width of up to 2 Å (Bystroff et al., 1990; Bystroff & Kraut, 1991). Such types of movement, to various degrees, are found in most enzymes (Kempner, 1993). The phenomenon is so pervasive that a protein motions data base, cataloging protein motions published in the literature, has been constructed and is accessible on the Internet (Gerstein et al., 1994). We would like to understand the mechanism, dynamics, and catalytic role of these types of movements.

Reaction Pathway of *E. coli* DHFR

$$E^{NADPH} \rightarrow E\frac{NADPH}{DHF} \rightarrow E\frac{NADPH}{DHF}^{\ddagger} \rightarrow E\frac{NADP^+}{THF} \rightarrow E_{THF} \rightarrow E\frac{NADPH}{THF} \rightarrow$$

Crystallized Reaction Pathway Analogues

C2	E^{NADPH}	$E\frac{NADP^+}{FOL}$	$E\frac{NADP^+}{MTX}$			
$P2_1$		$E\frac{NADP^+}{FOL}$	$E\frac{NADP^+}{MTX}$			
$P2_12_12_1^A$	E^{NADP^+}			$E\frac{NADP^+}{ddTHF}$		
$P2_12_12_1^B$	E^{NADPH}	$E\frac{NADP^+}{FOL}$	$E\frac{NADPH}{MTX}$	$E\frac{ATP-ribose}{ddTHF}$	E_{ddTHF}	$E\frac{NADPH}{ddTHF}$
$P3_221$	E^{NADPH}	$E\frac{NADP^+}{FOL}$	$E\frac{NADPH}{MTX}$			
$P6_1$					E_{ddTHF}	

FIGURE 1: Reaction pathway of ecDHFR: five detectable kinetic intermediates and the transition state for hydride transfer. Crystal structures representing these six points along the reaction pathway have been determined in multiple space groups. Only the crystal form $P2_12_12_1^B$ includes all six analogues in the same crystal packing.

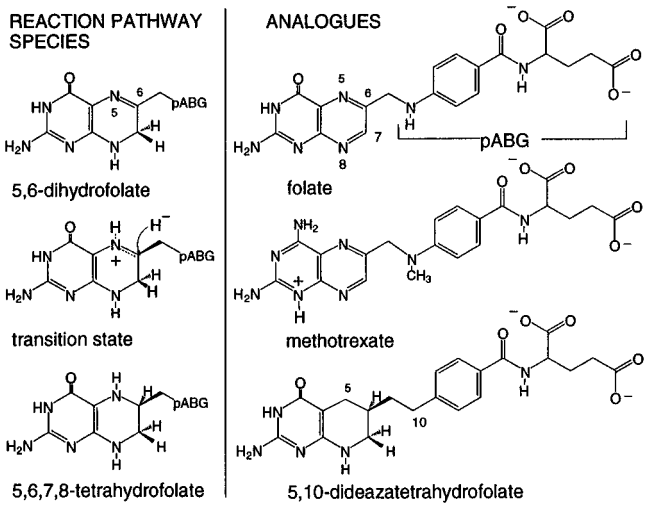

FIGURE 2: Chemical formulas for DHF, THF, the transition state for hydride transfer, and their analogues. MTX does not itself resemble the transition state, but its unique binding geometry induces the enzyme to adopt a conformation that thought to resemble the transition state.

However, it has been an ongoing struggle to correlate static structural detail with real time dynamics of the enzyme-catalyzed reaction, not just for ecDHFR but also for any enzyme molecule.

For a small group of enzymes, the connection between structural dynamics and kinetics has been made directly, employing time-resolved crystallography, a technically challenging experiment that allows observation of structural change during one turnover of substrate (Stoddard, 1996). While work is now in progress toward this goal for ecDHFR, in the meantime, isomorphous crystal structures (space group $P2_12_12_1^B$; see Table 1) have been determined that we believe reasonably well represent six points along the reaction coordinate, five kinetic intermediates on the predominant pathway, as well as the transition state (Figure 1). Specifically, these structures are ecDHFR complexes containing bound analogues of the kinetic intermediates. Analogues were used since actual intermediates are transient by nature and X-ray data collection by conventional methods requires several hours. The analogues employed are FOL for DHF in ternary complexes, MTX for the transition state of hydride transfer, ddTHF for THF, and ATP-ribose for $NADP^+$ when the nicotinamide moiety interfered with crystallization (Figure 2). We caution, however, that MTX does not itself resemble a transition state analogue, but according to previous structural studies, its unique binding geometry induces DHFR to adopt a conformation thought to resemble the transition state (Bystroff et al., 1990; Bystroff & Kraut, 1991).

The structures have been determined within a single crystal packing (space group $P2_12_12_1^B$) so that distortions due to crystal-packing effects remain constant for the series of structures [in contrast to previous crystallographic studies (Bystroff et al., 1990; Bystroff & Kraut, 1991)]. Molecular motions observed within this series of isomorphous structures are solely attributable to ligand-binding forces rather than to differences in crystal-packing forces. Furthermore, structures were also determined for subsets of the same six analogues in different crystal packings and space groups in order to (1) confirm the trends seen in $P2_12_12_1^B$ and (2) extrapolate our results on DHFR's conformational behavior in the crystal to DHFR's behavior in solution (Figure 1, Table 1). Since crystal-packing effects inevitably cause small local (and possibly global) deformations in protein molecules, examining the same complex within several different packing environments should provide a gauge of DHFR's range of behavior in solution. Examination of all these structures together has allowed us to propose herewith an approximate dynamical sequence, a detailed mechanism for conformational changes, and the catalytic relevance of loop and subdomain motions.

MATERIALS AND METHODS

Preparation of E. coli DHFR. Recombinant ecDHFR was purified from the RT500 strain of *E. coli* containing the plasmid PRWA-1 encoding DHFR. The plasmid and bacterial strain were gifts from Richard Wagner (University of Minnesota). The overexpression promotor has been described by Iwakura and Tanaka (1992). DHFR was purified by MTX affinity (Pierce, Rockford, IL) and DEAE-Sephacel ion exchange (Pharmacia, Piscataway, NJ) chromatography using procedures similar to those of Taira et al. (1987). More detailed procedures for cell growth, lysis, and purification are described in Sawaya (1994). Typically, twelve 1 L cultures yielded 500 mg of purified ecDHFR.

Preparation of E. coli DHFR Complexes. DHFR complex structures reported in this work are noted in Table 1. Due to the poor solubility of FOL, MTX (Sigma Chemical Co., St. Louis, MO), and ddTHF (Eli Lilly & Co., Indianapolis, IN), these ligands were added to apoenzyme when the DHFR concentration was relatively dilute, ≈1.0 mg/mL. The complex was concentrated to 30−40 mg/mL using Centricon-10 centrifugal microconcentrators (Amicon Corp., Beverly, MA). Cofactor [NADPH, $NADP^+$, or ATP-ribose (Sigma Chemical Co.)] could be added directly to the concentrated protein because it is sufficiently soluble. A 3-fold molar excess of ligand with respect to DHFR was used to ensure complex formation.

Crystallization Conditions. All crystals were grown using the standard sitting drop vapor diffusion method in MVD/24 crystallization plates (Charles Supper Co., Natick, MA), sealed with ordinary clear packaging tape (Manco Inc., purchased from Sears). Reservoirs contained 0.5 mL of

solution. The primary difficulty of this project was to crystallize analogues of five enzymic intermediates and the transition state *in the same space group and crystal packing*. Seven new crystalline forms were discovered. The most recent discovery of a new crystal form in space group $P2_12_12_1{}^B$, accommodating all six analogues, allowed the experiment to be completed (Table 1).

Crystallization in Space Group C2. Crystals in space group *C*2 grew within a week of macroseeding at room temperature. They typically reached dimensions of 1.0 × 0.4 × 0.2 mm. Crystals of binary complexes were thinner than those of ternary complexes. They contain one molecule per asymmetric unit.

ecDHFR·$NADP^+$/NADPH crystals were prepared by mixing 5 μL of ecDHFR·$NADP^+$ or ecDHFR·NADPH in 20 mM imidazole, at pH 7.0 with 5 μL of a reservoir solution containing 30% (w/v) PEG 6000, 11 mM $CaCl_2$, and 18 mM KHP at pH 6.0.

ecDHFR·FOL·ATP-ribose and ecDHFR·FOL·$NADP^+$ crystals were prepared by mixing 5 μL of either ecDHFR·FOL·ATP-ribose or ecDHFR·FOL·$NADP^+$ in 20 mM imidazole at pH 7.0 with 5 μL of a reservoir solution containing 32% (w/v) PEG 6000 and 10 mM $CaCl_2$.

ecDHFR·MTX·$NADP^+$ crystals were prepared by mixing 5 μL of ecDHFR·MTX·$NADP^+$ in 10 mM imidazole at pH 7.0 with 5 μL of a reservoir solution containing 30% (w/v) PEG 6000, 30 mM KHP (pH 6.0), and 11 mM $CaCl_2$.

Crystallization in Space Group $P2_1$. Crystals in space group $P2_1$ grew within 1 week at room temperature, typically reaching a size of 0.6 × 0.5 × 0.1 mm. They contain two molecules per asymmetric unit.

ecDHFR·FOL·$NADP^+$ crystals were prepared by mixing 5 μL of ecDHFR·FOL·$NADP^+$ in 20 mM imidazole at pH 7.0 with 5 μL of a reservoir solution containing 25% (w/v) PEG 6000, 90 mM $CaCl_2$, and 60 mM Tris at pH 8.0.

ecDHFR·MTX·$NADP^+$ crystals were prepared by mixing 5 μL of ecDHFR·MTX·$NADP^+$ in 20 mM imidazole at pH 7.0 with 5 μL of a reservoir solution containing 25% (w/v) PEG 6000, 50 mM $CaCl_2$, and 60 mM imidazole at pH 7.2.

Crystallization in Space Group $P2_12_12_1{}^A$. ecDHFR·ddTHF·$NADP^+$ crystals in space group $P2_12_12_1{}^A$ grew within 1 week at room temperature, typically reaching a size of 0.8 × 0.5 × 0.2 mm. They contain one molecule per asymmetric unit and are isomorphous with the previously described ecDHFR·$NADP^+$ crystals (Bystroff et al., 1990).

ecDHFR·ddTHF·$NADP^+$ crystals were prepared by mixing 5 μL of ecDHFR·ddTHF·$NADP^+$ in 20 mM imidazole at pH 7.0 with 5 μL of a reservoir solution containing 25% (w/v) PEG 6000, 50 mM $CaCl_2$, and 60 mM imidazole at pH 7.2.

Crystallization in Space Groups $P2_12_12_1{}^{B,E}$. Crystals in space group $P2_12_12_1{}^B$ grew within 1 week of macroseeding at 4 °C. They typically reached a size of 0.6 × 0.4 × 0.2 mm. They contain one molecule per asymmetric unit.

ecDHFR·ddTHF crystals were prepared by mixing 5 μL of ecDHFR·ddTHF·$NADP^+$ in 20 mM imidazole at pH 7.0 with 5 μL of a reservoir solution containing 16% (w/v) PEG 6000, 300 mM $MnCl_2$, and 20 mM imidazole at pH 7.4. These crystals were the result of failed attempts at a ternary complex.

ecDHFR·FOL crystals were prepared by mixing 5 μL of ecDHFR·FOL in 20 mM cacodylate at pH 7.0 with 5 μL of a reservoir solution containing 20% (w/v) PEG 6000, 300 mM $MnCl_2$, and 20 mM cacodylate at pH 6.5.

ecDHFR·$NADP^+$ crystals were prepared by mixing 3 μL of ecDHFR·$NADP^+$ in 10 mM imidazole at pH 7.0 with 3 μL of a reservoir solution containing 15% (w/v) PEG 6000, 300 mM $CaCl_2$, and 100 mM imidazole at pH 6.0.

ecDHFR·NADPH crystals were prepared by mixing 3 μL of ecDHFR·NADPH in 10 mM imidazole at pH 8.0 with 3 μL of a reservoir solution containing 25% (w/v) PEG 6000, 450 mM $CaCl_2$, and 100 mM imidazole at pH 8.0. A strongly buffered pH 8.0 solution was used in order to prevent hydration of the nicotinamide ring (Oppenheimer, 1982), which is detectable by measuring UV absorbance at 340 nm. Immediately after a crystal was selected for data collection, another crystal taken from the same drop was dissolved and its UV absorbance spectrum was measured. The spectrum indicated that NADPH was fully reduced at the time of data collection. Following 18 h of data collection, the X-rayed crystal was dissolved in 10 mM imidazole at pH 8.0 and its UV absorbance spectrum was measured. Peak absorbance at 340 nm characteristic of the reduced nicotinamide ring had disappeared, possibly due to X-ray-generated oxidation of the nicotinamide.

ecDHFR·ddTHF·ATP-ribose crystals were prepared by mixing 5 μL of ecDHFR·ddTHF·ATP-ribose in 20 mM imidazole at pH 7.0 with 5 μL of a reservoir solution containing 20% (w/v) PEG 6000, 300 mM $CaCl_2$, and 20 mM cacodylate at pH 6.0.

ecDHFR·ddTHF·NADPH crystals were prepared by mixing 5 μL of ecDHFR·ddTHF·NADPH in 20 mM imidazole at pH 7.0 with 5 μL of a reservoir solution containing 20% (w/v) PEG 3350, 300 mM $CaCl_2$, and 100 mM imidazole at pH 6.0.

ecDHFR·FOL·ATP-ribose and ecDHFR·FOL·$NADP^+$ crystals were prepared by mixing 5 μL of either ecDHFR·FOL·ATP-ribose or ecDHFR·FOL·$NADP^+$ in 20 mM imidazole at pH 7.0 with 5 μL of a reservoir solution containing 16% (w/v) PEG 6000, 300 mM $MnCl_2$, and 20 mM imidazole at pH 7.0.

ecDHFR·MTX·NADPH crystals were prepared by mixing 5 μL of ecDHFR·MTX·NADPH in 20 mM imidazole at pH 7.0 with 5 μL of a reservoir solution containing 23% (w/v) PEG 6000, 300 mM $MnCl_2$, and 20 mM imidazole at pH 7.0.

ecDHFR·DHF crystals in space group $P2_12_12_1{}^E$ were prepared by mixing 5 μL of ecDHFR·DHF in 20 mM imidazole at pH 7.0 with 5 μL of a reservoir solution containing 16% (w/v) PEG 6000, 210 mM $MnCl_2$, and 20 mM KHP at pH 6.6. These crystals differed in morphology and unit cell dimensions from those of $P2_12_12_1{}^B$ but have similar packing interactions. A 10-fold molar excess of DHF with respect to DHFR resulted in the observation of a second ordered molecule of DHF found outside the active site, near C152.

Crystallization in Space Groups $P2_12_12_1{}^{C,D}$. Crystals in space groups $P2_12_12_1{}^{C,D}$ grew within 1 week at room temperature. Differences in pH and metal ion produced these two crystal forms with similar though nonisomorphous unit cell parameters and packings. Both contain two molecules per asymmetric unit.

ecDHFR·FOL crystals in $P2_12_12_1{}^C$ were prepared by mixing 5 μL of ecDHFR·FOL in 10 mM imidazole at pH 7.0 with 5 μL of a reservoir solution containing 30% (w/v) PEG 6000, 200 mM monosodium glutamate, and 100 mM Tris at pH 8.5.

ecDHFR·FOL crystals in $P2_12_12_1{}^D$ were prepared by mixing 5 μL of ecDHFR·FOL in 10 mM imidazole at pH

Table 2: Data Collection and Refinement Statistics for *E. coli* DHFR Structures

	data collection						refinement		
							rms deviation		
complex	space group	d_{min} (Å)	I^a/σ	total observations/ unique reflections	completeness (%)	$R_{sym}{}^b$	bond (Å)	angle (deg)	final^c R
$NADP^+$	$C2$	1.5	2.0	75470/22697	95	0.048	0.021	3.0	0.169
NADPH		1.9	2.9	30974/12031	96	0.035	0.013	2.9	0.147
FOL·ATP-ribose		1.8	2.7	32887/10657	72	0.038	0.022	3.0	0.144
FOL·$NADP^+$		1.6	2.3	63457/20384	95	0.042	0.022	3.0	0.171
MTX·$NADP^+$		1.8	3.3	32985/13431	95	0.040	0.020	3.0	0.170
FOL·$NADP^+$	$P2_1$	2.1	2.0	72595/20914	87	0.098	0.013	3.0	0.205
MTX·$NADP^+$		2.3	2.1	45132/14094	96	0.096	0.014	2.9	0.160
ddTHF·$NADP^+$	$P2_12_12_1{}^A$	1.9	2.0	38211/14235	93	0.052	0.017	2.9	0.179
ddTHF	$P2_12_12_1{}^B$	2.3	1.9	21289/6930	93	0.075	0.021	3.0	0.174
FOL		2.3	2.1	13988/6569	87	0.078	0.022	3.0	0.181
$NADP^+$		1.9	2.1	37929/11575	90	0.097	0.021	3.0	0.184
NADPH		2.0	2.1	35340/11692	92	0.129	0.019	3.0	0.180
ddTHF·ATP-ribose		2.2	2.4	25388/8166	95	0.076	0.020	2.9	0.175
ddTHF·NADPH		2.0	1.8	40855/10505	92	0.113	0.021	3.0	0.184
FOL·ATP-ribose		2.8	1.8	12117/3835	92	0.097	0.020	2.8	0.144
FOL·$NADP^+$		1.8	2.0	64582/14178	94	0.091	0.022	3.0	0.171
MTX·NADPH		2.2	2.0	35193/8086	97	0.087	0.020	2.9	0.156
FOL	$P2_12_12_1{}^C$	2.6	1.8	53453/12108	99	0.090	0.023	2.9	0.163
FOL	$P2_12_12_1{}^D$	2.6	2.1	35221/9448	88	0.093	0.020	2.7	0.178
DHF	$P2_12_12_1{}^E$	1.8	2.2	38377/14125	96	0.048	0.015	2.8	0.170
MTX	$P2_12_12_1{}^F$	2.0	2.1	35093/11593	86	0.042	0.031	2.9	0.170
NADPH	$P3_221$	2.3	2.1	42407/10655	90	0.048	0.020	3.0	0.201
MTX·$NADP^+$		2.6	2.3	29632/7357	93	0.055	0.016	2.8	0.216
MTX·NADPH		2.4	2.9	36699/9577	94	0.057	0.020	3.0	0.228

^{a} Average ratio of observed intensity to σ in the highest-resolution shell of reflections. ^{b} $R_{sym} = \sum|I_{obs} - I_{avg}|/\sum I_{avg}$. ^{c} Final $R = \sum|F_{obs} - F_{calc}|/\sum F_{obs}$, including all data between 20 Å and the maximum resolution.

7.0 with 5 μL of a reservoir solution containing 26% (w/v) PEG 6000, 200 mM $MgCl_2$, and 100 mM Tris at pH 8.0.

Crystallization in Space Group $P2_12_12_1{}^F$. ecDHFR·MTX crystals in space group $P2_12_12_1{}^F$ grew after 4 months, reaching a size of 0.4 × 0.4 × 0.4 mm. Crystals were prepared by mixing 5 μL of ecDHFR·MTX·$NADP^+$ in 20 mM imidazole at pH 7.0 with 5 μL of a reservoir solution containing 25% (w/v) PEG 6000, 50 mM $CaCl_2$, and 60 mM imidazole at pH 7.2. Although grown in the presence of $NADP^+$, no $NADP^+$ appeared in the final structure.

Crystallization in Space Group $P3_221$. Crystals in space group $P3_221$ were grown at 4 °C and required a 40−50 mg/mL concentration of DHFR. White cloudy precipitate appeared immediately after mixing the drop. The precipitate usually dissolved within the next 2 days to give a single crystal. They typically grew to a size of 1.0 × 0.8 × 0.6 mm and are isomorphous with respect to ecDHFR·FOL·-$NADP^+$ crystals reported by Bystroff et al. (1990).

ecDHFR·NADPH crystals were prepared by mixing 15 μL of ecDHFR·NADPH in 10 mM imidazole at pH 7.0 with 3.5 μL of a solution containing 30% (w/v) PEG 6000, 2% ethanol, and 27 mM $CaCl_2$. The reservoir contained 500 μL of 25% PEG 6000, 2% ethanol, and 27 mM $CaCl_2$. Seeds were obtained from drops with slightly higher PEG concentrations (≈27−30%) and were washed in reservoir solution to remove microseeds.

ecDHFR·MTX·$NADP^+$ crystals were prepared by mixing 12 μL of ecDHFR·MTX·$NADP^+$ in 50 mM KHP at pH 6.0 with 5 μL of 50% (w/v) PEG 6000 and 1.5 μL of 50 mM $CaCl_2$. The reservoir contained 500 μL of 12% PEG 6000, 3% ethanol, and 50 mM KHP at pH 6.0.

ecDHFR·MTX·NADPH crystals were prepared by mixing 14 μL of ecDHFR·MTX·NADPH in 10 mM imidazole at pH 7.0 with 7 μL of a solution containing 29% (w/v) PEG 6000 and 12 mM $CaCl_2$. The reservoir contained 500 μL of 20% PEG 6000 and 40 mM $CaCl_2$. Macroseeding was required.

Crystallization in Space Groups $P6_1$ and $P6_5$. Crystallization conditions for ecDHFR·MTX in space group $P6_1$ have been reported by Matthews et al. (1977). Since then, isomorphous complexes of ecDHFR·5-deazafolate, ecDHFR·-ddTHF, and ecDHFR·FOL have been reported by Reyes et al. (1995). Conditions for growing ecDHFR·folinic acid crystals in $P6_1$ and $P6_5$ have been reported in Lee et al. (1996).

Data Collection and Structure Determination. All X-ray diffraction data were collected at room temperature or 4 °C using a Rigaku-RU300 Cu rotating anode equipped with Xuong-Hamlin multiwire area detectors (Hamlin, 1985) (Table 2). Data were reduced using University of California, San Diego, data collection software (Howard et al., 1985). The Merlot molecular replacement package (Fitzgerald, 1988) was used to determine initial sets of phases in space groups $C2$, $P2_1$, and $P2_12_12_1{}^{B,C,D,E,F}$. The rotation and translation solutions for all seven space groups were 5σ or higher and unambiguous. Structures were then refined using the TNT least-squares refinement program (Tronrud et al., 1987). All structures were refined with good geometry (rms deviation in bond lengths of 0.020−0.021 Å, rms deviation in bond angles of 2.9−3.1°) and an acceptable R factor (Table 2), with the possible exception of the $P3_221$ structures, which characteristically suffered from relatively high R factors (20−23%) and a high overall temperature factor. These problems are most likely due to static disorder. The high R factor and temperature factors were *not* the result of an intermolecular disulfide bridge (Cys 152) between two asymmetric units as suggested by Bystroff et al. (1990). This disulfide was clearly reduced in the ecDHFR·MTX·NADPH structure, yet it retains the same poor refinement characteristics as the disulfide-cross-linked ecDHFR·MTX·$NADP^+$.

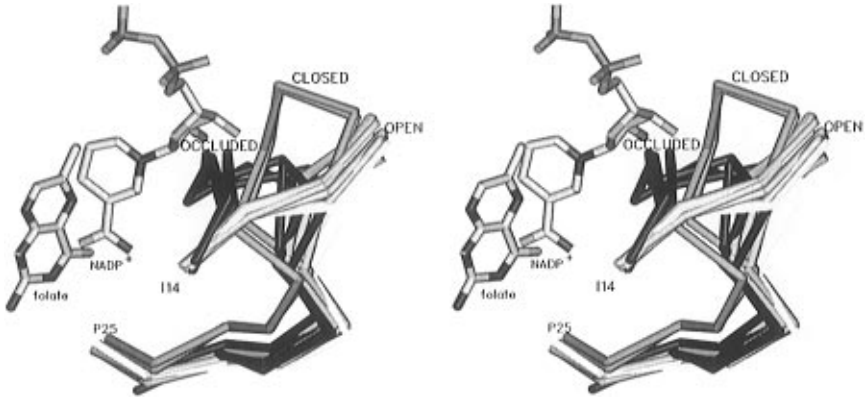

FIGURE 3: α-Carbon traces of the M20 loops from each crystal form in Table 1 (except $P2_12_12_1^F$ and $P3_121$ in which the loop is disordered). Only one ligated state is shown for each crystal form since there is no variation within any given form. The single exception is space group $P2_12_12_1^B$ in which the crystal lattice allows both closed and occluded conformations. α-Carbons of residues 1−13 and 26−159 were used for superpositioning. For reference, folate and $NADP^+$ are drawn in their proper binding pockets. In the occluded conformation, the M20 loop protrudes into the nicotinamide−ribose binding pocket of $NADP^+$. The open conformation is clearly the most common. The sequence of the loop (residues 10−24) is VDRVIGMENAMPWNL. This figure was produced using the graphics program Setor (Evans, 1993).

RESULTS AND DISCUSSION

General Description of ecDHFR Structure and Flexibility. All structurally determined, chromosomally encoded DHFRs are single-domain, monomeric molecules containing a mixed, eight-stranded β-sheet (strands βA−βH); all strands are parallel except for the C-terminal antiparallel strand, βH. The sheet is flanked by four α-helices (B, C, E, and F), two helices on either side of the sheet. Because the structural unit comprising strands B, C, D, and E plus helices C, E, and F behaves as a rigid body and binds the adenosine portion of NADP, it is termed the adenosine binding subdomain. The remaining structure, also a rigid body, is termed the loop subdomain because 45% of its sequence encodes the three principal loops: the M20 loop, the F−G loop, and the G−H loop.[2] A gap separating the two subdomains is formed by a break in the hydrogen-bonding pattern between strands A and E. The nicotinamide ring, coplanar with the sheet, spans this gap, while the pteridine ring is juxtaposed at a 45° angle, fitting into a cleft between helices B and C. The hydride donor (C4 of NADPH) and hydride acceptor (C6 of DHF) are held in sub van der Waals contact in the ground state. The reactants are shielded from solvent when a flexible, largely conserved, ω-type loop termed the M20 loop in ecDHFR (residues 10−24) closes over the active site. Loop movement and rotation between the two subdomains are the two major features of conformational flexibility observed in ecDHFR.

Conformations of the M20 Loop; Four Classes. During the 1970s and 1980s, crystallographic studies of DHFR revealed four conformational states of the M20 loop. Three of the states have since been classified as the open, closed, and occluded conformations, according to whether the active site is open, closed, or occluded by the loop. The fourth state, the disordered state, describes cases in which motion renders the loop crystallographically unclear or invisible. Now, five years after our last report dealing with conformational movements (Bystroff & Kraut, 1991), 8 new crystal forms and over 40 new ecDHFR structures have been analyzed, yet this conformational repertoire remains unchanged. As is readily apparent in Figure 3, ordered loops from all known ecDHFR crystal structures cluster around three conformations: open, closed, and occluded. Main chain torsion angles of the three conformations vary widely in the N-terminal and central portion of the loop (residues 14−19), with lesser variation near the C-terminal end (residues 20−25). But, among members of the same class, there is a rather low rms deviation in Cα positions despite differences in the crystal packing and the ligated state.

The four loop conformations are best characterized by their secondary structure, interactions with nicotinamide−ribose, and hydrogen-bonding patterns with neighboring loops (F−G and G−H loops). Ranked by these characteristics, the closed and occluded conformations lie on either end of a spectrum, while the open conformation displays intermediate characteristics. The disordered conformation displays characteristics of a time-averaged exchange of closed and occluded conformations.

The closed conformation is observed in complexes crystallizing in space groups $P2_12_12_1^B$ ($NADP^+$, NADPH, FOL·$NADP^+$, and MTX·NADPH) and $P3_221$. It is also the sole conformation observed in DHFRs from all other sources, including vertebrate DHFRs, *P. carinii*, *L. major*, and *La. casei*, regardless of the ligated state and crystal packing. The center of the loop forms a short antiparallel sheet and type III′ hairpin turn (residues 16−19) (Figure 4A) which extends across and seals the active site by placing N18(Nε1) of the hairpin in position to form a hydrogen bond with H45(O) of helix C. This conformation interacts closely with the nicotinamide−ribose of NADP via a hydrogen bond with the nicotinamide's carboxamide group [NADP(NN7)−I14-(O)] and van der Waals contacts between the ribose and backbone of N18 and A19 and the side chain of M20 (Figures 5A and 6A). A pair of hydrogen bonds with the F−G loop [G15(O)−D122(N) and E17(N)−D122(Oε2)] help maintain the conformation of the N-terminal end of the loop (Figure 5A). Conversely, the C-terminal end of the loop is disengaged from a pair of hydrogen bonds with the G−H loop (Figure 6A), which if formed would favor the occluded conformation (see below).

The occluded conformation, the opposite conformational extreme, is observed in complexes crystallizing in space

[2] We use the term "subdomain" rather than "domain" which was used by Bystroff and Kraut (1991) because we believe that the two subdomains compose the single domain of DHFR. Also, in view of new evidence, the assigned composition of the two subdomains has been modified. Hence, the name "major subdomain" was changed to "loop domain" since it is a more descriptive term and because its size no longer warrants the adjective major (see below).

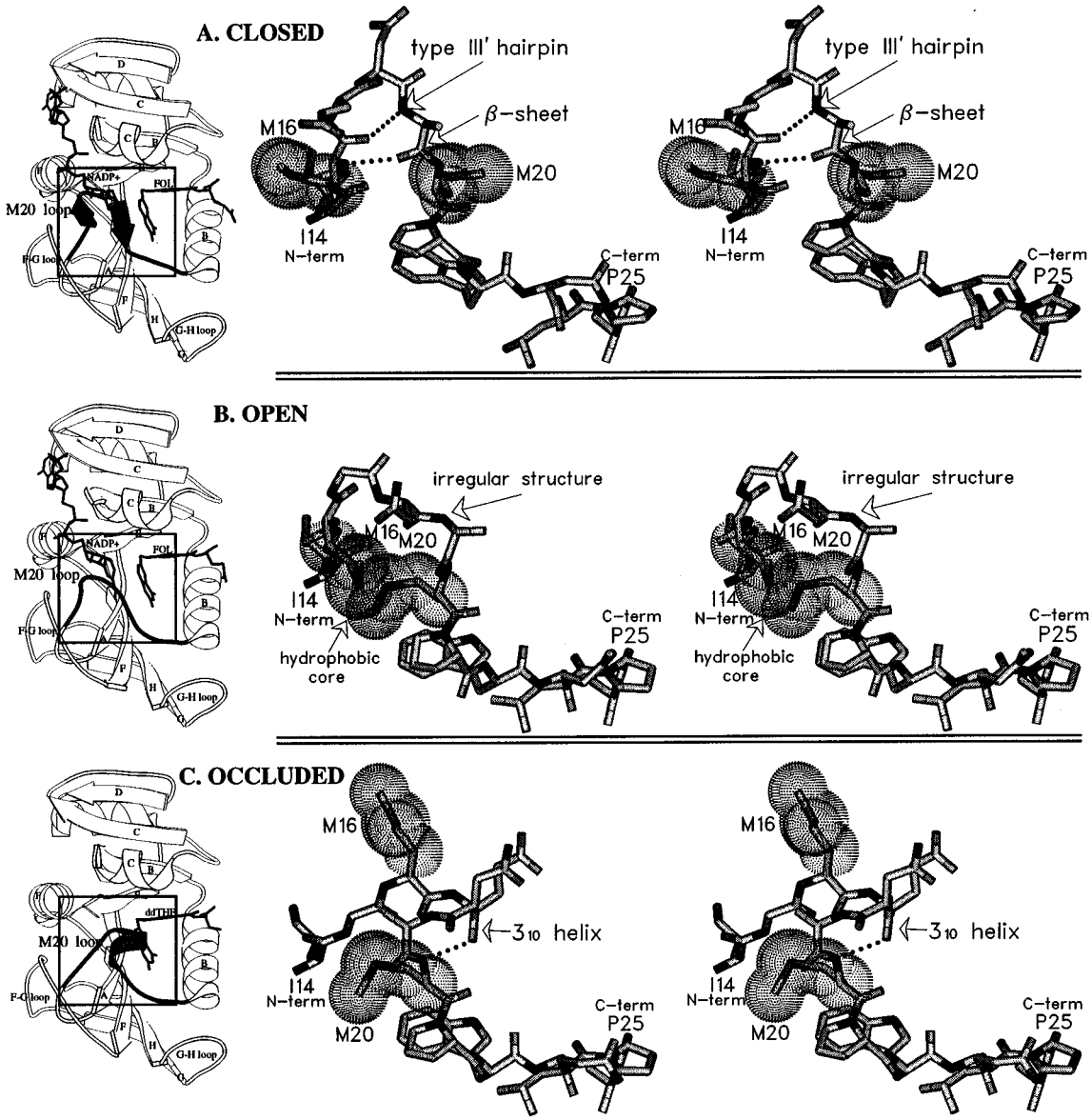

FIGURE 4: Central view of M20 loops in the (A) closed, (B) open, and (C) occluded conformations. van der Waals surfaces are drawn for the side chains of M16 and M20 illustrating the formation of a hydrophobic contacts in the open conformation. Note that the N-terminal side of the M20 loop is bordered by the F−G loop and the C-terminal side of the M20 loop is bordered by the G−H loop. This figure was produced using the graphics programs Setor (Evans, 1993) and Molscript (Kraulis, 1991).

groups $P2_12_12_1^B$ (ddTHF, FOL, ddTHF·ATP-ribose, ddTHF·-NADP$^+$, and ddTHF·NADPH), $P2_12_12_1^E$, $P6_1$ (molecule A), and $P6_5$. Instead of a β-sheet/hairpin, the central part of the loop (E17−M20) forms a 3_{10} helix (Figure 4C).[3] In contrast to the closed conformation, the occluded conformation inhibits cofactor binding by occluding the nicotinamide binding pocket (Figures 5C and 6C). A 180° rotation about ψ^{I14} directs the N-terminal end of the loop into the nicotinamide binding pocket and puts M16 in van der Waals contact with T46 and S49 (Figure 6C). Redirection of the N-terminal end of the loop also completely disrupts hydrogen bonds with the F−G loop, while the C-terminal end of the loop forms strong hydrogen bonds with the G−H loop [N23(O)−S148(N), 2.8 Å; N23(N)−S148(Oγ), 2.8 Å] (Figure 6C). The latter pair of hydrogen bonds require that the C-terminal end of the loop and the N-terminal end of helix B shift ≈0.5 Å closer to the G−H loop.

The open conformation, the most frequently occurring conformation crystallographically, is observed in all complexes in space groups $C2$, $P2_1$ (molecules A and B), $P2_12_12_1^{C,D}$ (molecules A and B), and $P6_1$ (molecule B). Its structural characteristics suggest that it resembles an intermediate state between the closed and occluded conformations. Individual main chain torsion angles correspond to either the closed form or the occluded form, with the single exception of ψ^{N18} which deviates significantly from both. The mixture of torsion angles results in an irregular conformation with no internal hydrogen bonds or regular secondary structure. Instead, M16 and M20 side chains rotate inward, forming stabilizing hydrophobic contacts within the loop (Figure 4B). The open loop's apparent affinity for cofactor would be intermediate between that of the closed and occluded forms. A single hydrogen bond is formed between I14(O) and nicotinamide NN7. The rest of the loop extends away from the reactants, allowing the nicotinamide−ribose into or out of its binding pocket. Moreover, the open loop's hydrogen bonds with the supporting F−G and G−H loops exhibit a pattern characteristic

[3] The 3_{10} helix is interrupted by lattice contacts in $P6_1$ (molecule A). In contrast, the helix is stabilized by Ca^{2+} binding to the helix's C terminus in $P6_5$. However, cation binding appears adventitious because the 3_{10} helix forms just as well in the absence of bound Ca^{2+} ($P2_12_12_1^B$).

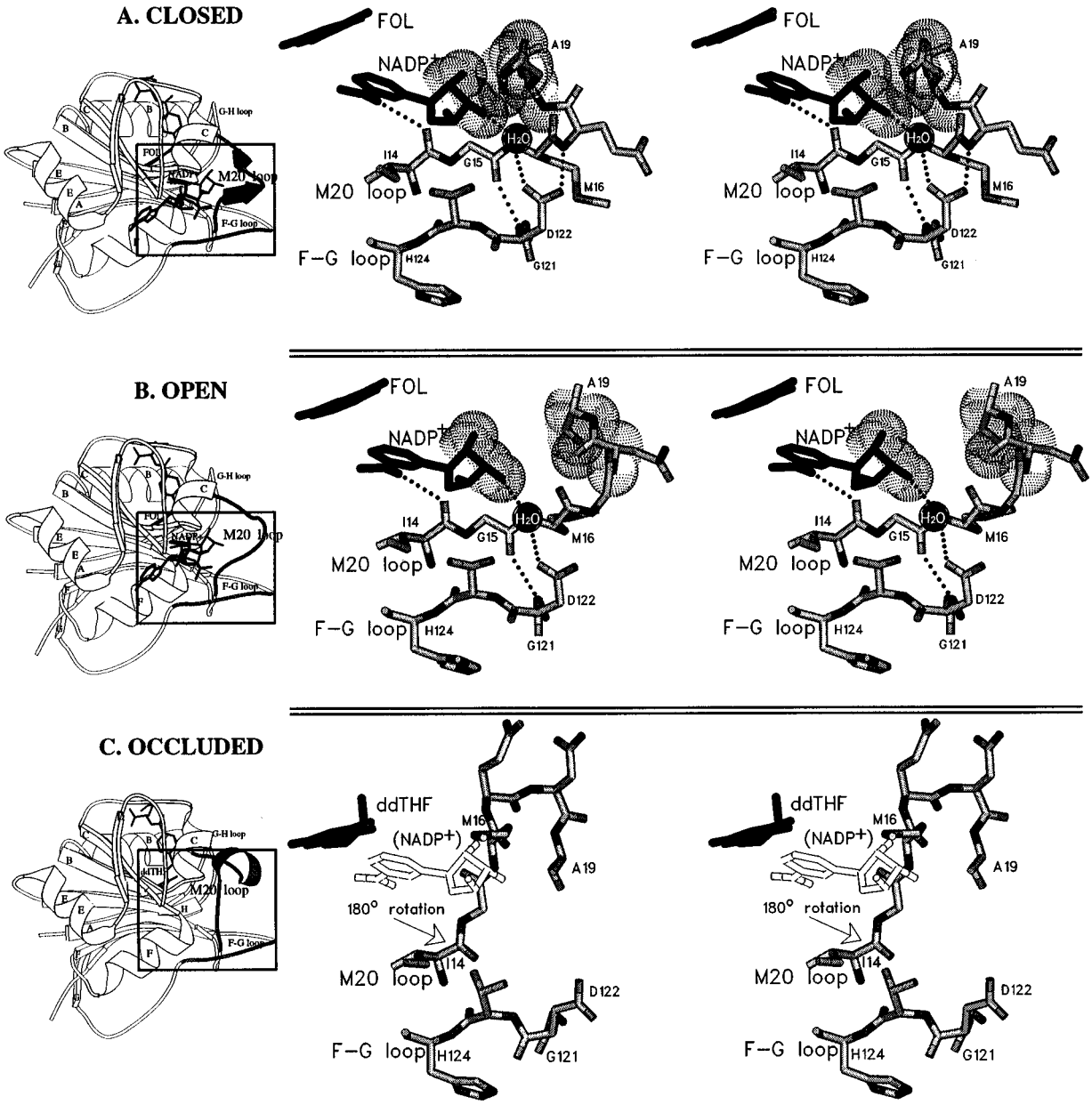

FIGURE 5: View of F−G loop interactions with M20 loops in (A) closed, (B) open, and (C) occluded conformations. van der Waals surfaces are drawn for $NADP^+$'s ribose and contacting backbone atoms of N18-A19 in the closed conformation. In the open conformation, there is no contact between ribose and N18-A19. A hydrogen bond between the nicotinamide's carboxamide NN7 and I14(O) is indicated in the closed and open conformations. The occluded conformation's ψ_{I14} labeled in C, is 180° away from that of the closed or open conformations, directing the M20 loop into the nicotinamide−ribose binding pocket. The nicotinamide cannot bind in the occluded conformation, but its outline has been drawn to indicate how it would clash with M16. Most importantly, note the hydrogen bonds between G15(O) and D122(N) and E17(N) and D122(Oϵ2) in the closed and open conformations but *not* in the occluded conformation. This figure was produced using the graphics programs Setor (Evans, 1993) and Molscript (Kraulis, 1991).

of both the closed and occluded loops. Like that of the closed conformation, the N terminus of the open loop forms a pair of hydrogen bonds with the F−G loop (ψ^{I14} is not flipped over) (Figure 5B). Like that of the occluded conformation, the C terminus of the open loop forms a pair of hydrogen bonds with the G−H loop (Figure 6B).

If the open conformation is indeed an intermediate between closed and occluded forms of the M20 loop, it may be expected that the open conformation be physically between the closed and occluded conformations. Upon inspection of Figure 3, this is clearly not the case; the open conformation extends outside the closed and occluded conformations. But because movement between closed and occluded forms of the M20 loop entails large rotations of several main chain torsion angles, not a simple rotation on two hinges, the path of loop motion is not limited to being within the boundaries of the closed and occluded loop conformations, especially in the central portion where change is greatest.

Disordered loops are observed in space groups $P2_12_12_1^F$ (MTX complex) and $P3_121$ (apoenzyme). Consistent with the idea that the disordered form may result from a time-averaged interconversion between the closed and occluded conformations, the degree of disorder observed in electron density maps corresponds to the distance in atomic position between closed and occluded forms. Further, rotation about ψ^{I14}, required for interconversion between closed and occluded forms, appears to be responsible for a precipitous drop in electron density following I14. No hydrogen bonds are observed with the F−G loop [G15(O)−D122(N) and E17(N)−D122(Oϵ2)], as G15 and E17 are invisible due to the disorder. The F−G loop also displays high temperature factors and some disordered side chains in this region,

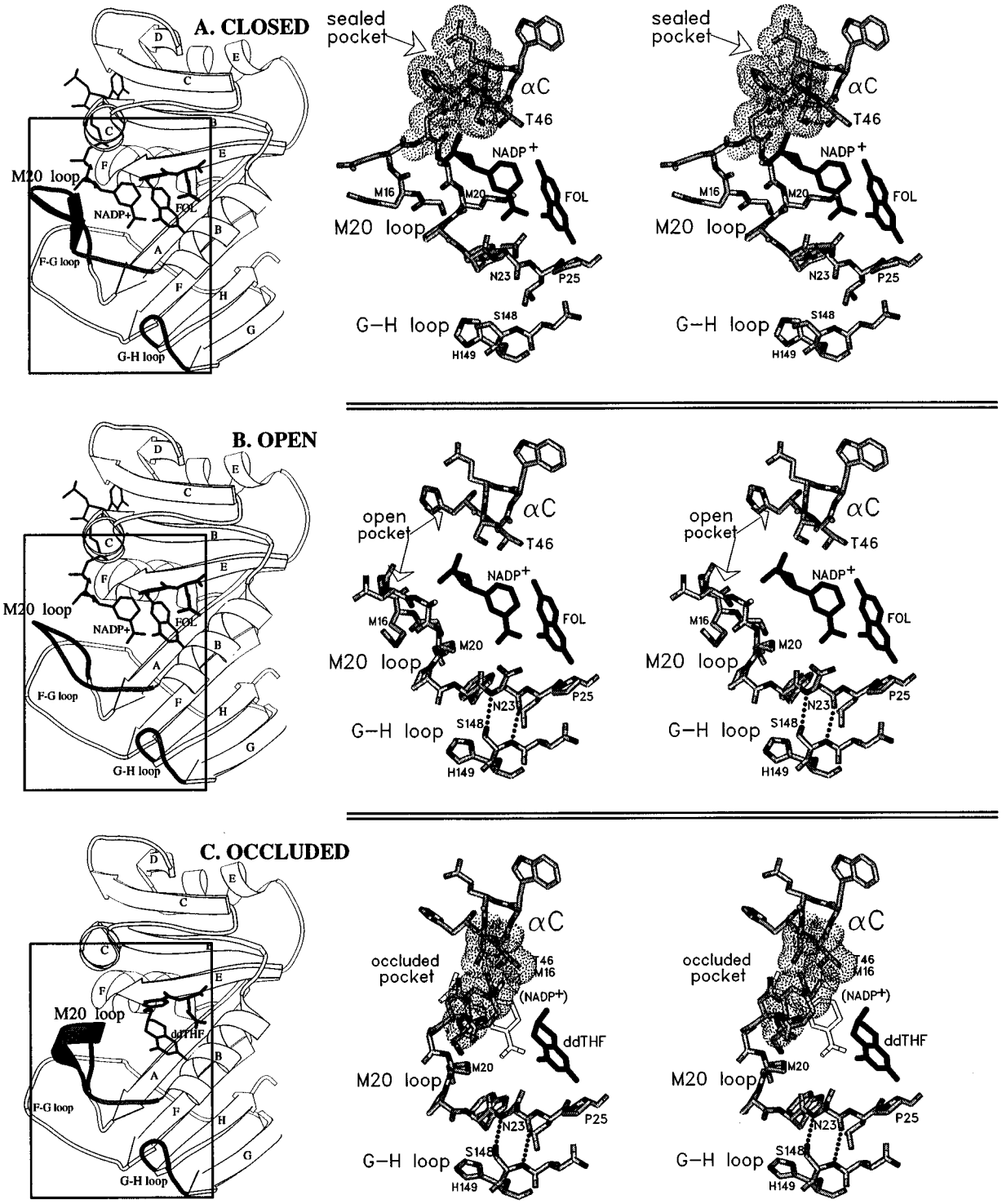

FIGURE 6: View of G−H loop interactions with M20 loops in (A) closed, (B) open, and (C) occluded conformations. van der Waals surfaces are drawn showing how access to the nicotinamide binding pocket is altered. In the closed form, the pocket is sealed, and in the open form, there is an 8 Å gap; while in the occluded conformation, M16 occludes the pocket. Most importantly, note the hydrogen bonds between N23(O) and S148(N) and N23(N) and S148(Oγ) in the open and occluded conformations but *not* in the closed conformation. This figure was produced using the graphics programs Setor (Evans, 1993) and Molscript (Kraulis, 1991).

indicating that it, too, is moving. A pair of hydrogen bonds with the G−H loop are also broken. Of the remaining ordered M20 loop residues, there are no contacts with MTX.

There is another group of structures that display a less severe type of disorder. In these cases, the M20 chain is traceable, though the average temperature factor of the main chain is over 40 Å^2. This type of disorder is visible in the occluded conformations of space groups $P2_12_12_1^{A,B}$ and the closed conformation of NADP$^+$ and NADPH complexes in $P2_12_12_1^{B}$. Motion of this type may be due to interconversion between closed and occluded conformations (see below).

Influence of Crystal Packing on Loop Conformation. In most crystal forms, there is no variation in loop conformation within a series of isomorphous structures, regardless of the ligated state. The cause of immobilization can be traced to crystal lattice contacts at one or more of the three principal loops: the M20 loop, the F−G loop, or the G−H loop. These contacts evidently shift the equilibrium in favor of one particular conformation. When the loop is closed (space group $P3_221$), crystal contacts between the G−H loop and the C−D loop of another symmetry-related molecule destabilize the occluded conformation by preventing formation of a pair of

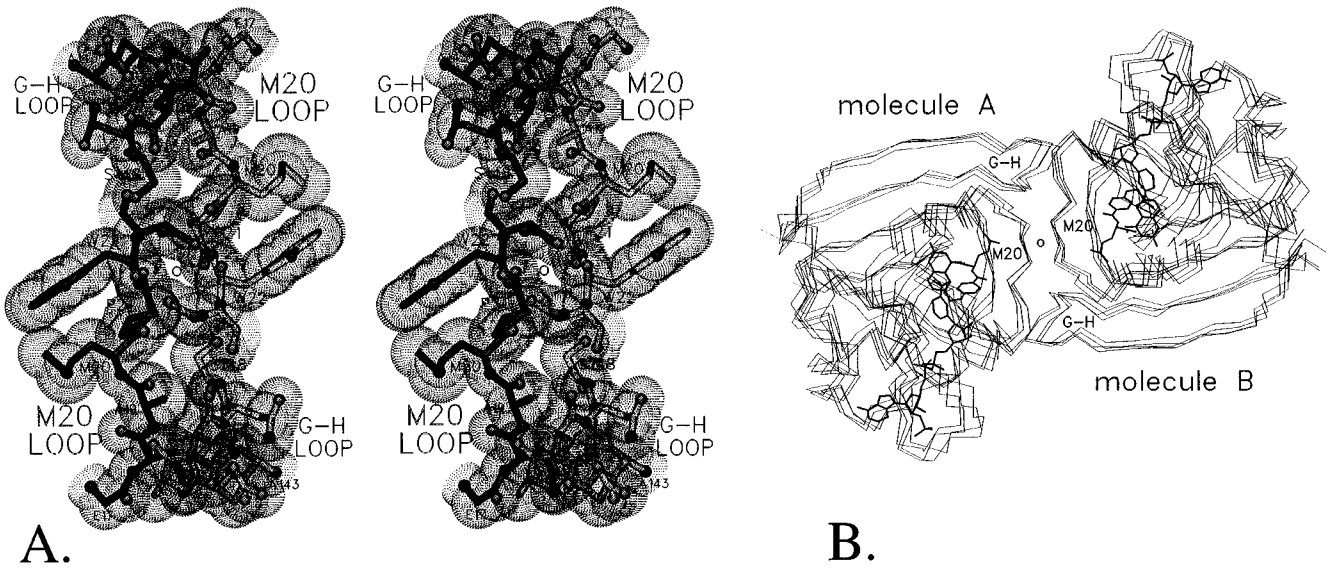

FIGURE 7: (A) Extensive interactions between M20 loops of 2-fold symmetry-related molecules. This packing is characteristic of all open loop conformations, regardless of crystal form. (B) Superposition of the dimers shows how well the intermolecular contacts are conserved. DHFR molecules in (A) and (B) are shown in the same orientation. This figure was produced using the graphics program Setor (Evans, 1993).

interloop hydrogen bonds with the M20 loop [N23(O)−S148(N) and N23(N)−S148(Oγ)]. When the loop is open, as in space groups $P2_12_12_1^{C,D}$, $P6_1$ (molecule B), $P2_1$, and $C2$, there are extensive contacts between $P21$ and W22 of one molecule, and the $P21$ and W22 of a two-fold symmetry related molecule (Figure 7A). The symmetry-generated contacts are so well conserved that pairs of ecDHFR molecules from the different space groups can be superposed as rigid dimers (Figure 7B). When the loop is in the occluded form, as in space groups $P6_1$ (molecule A) and $P6_5$, crystal contacts with the F−G loop destabilize formation of the closed conformation by preventing formation of a pair of interloop hydrogen bonds with the M20 loop [G15(O)−D122(N) and E17(N)−D122(Oϵ2)]. In space groups where the loop appears mobile ($P2_12_12_1^{A,B}$ and $P3_121$), there are few, weak lattice contacts in loop areas. Most notable is space groups $P2_12_12_1^B$ in which the loop changes from closed to disordered depending on the ligated state. Due to the absence of lattice interference with M20 loop mobility, M20 loop conformations observed in the analogue complexes in space groups $P2_12_12_1^{A,B}$ are regarded as indicators of conformational behavior in solution during a reaction cycle.

Loop Movement during the Reaction Cycle. Crystallographic evidence from the space group $P2_12_12_1^B$ structures (where loop movement is allowed by the crystal lattice) suggests that the closed conformation of the M20 loop is favored in the first half of the reaction cycle, *i.e.* in the holoenzyme, Michaelis complex, and transition state complex (Figure 8). The M20 loop conformation is ordered and closed in isomorphous crystal structures representing these complexes (NADPH, FOL·NADP$^+$, and MTX·NADPH complexes). ^{19}F and ^{1}H NMR also confirm that the M20 loop of FOL·NADP$^+$ and MTX·NADPH exists primarily in a single, well-defined conformation, indicated by strong NOEs between M20 and W22 (Hoeltzli & Frieden, 1994). The M20 loop in the NADPH crystal structure displays higher temperature factors than in the two ternary complexes (about 15 Å^2 higher on the average), consistent with the diminished resonance signal from labeled [6-^{19}F]W22 in the NADPH complex. During the second half of the reaction cycle, *i.e.* in the THF·NADP$^+$, THF, and THF·NADPH complexes, the occluded form appears to be favored (Figure 8). Crystal structures representing these complexes (ddTHF·ATP-ribose, ddTHF, and ddTHF·NADPH) reveal the occluded conformation, though temperature factors indicate substantial motion (average main chain temperature factors range from 41 to 53 Å^2).

Mechanism of M20 Loop Movement. Thermodynamic equilibrium between the closed and occluded conformations is shifted in favor of the closed conformation by binding of the nicotinamide−ribose moiety of NADPH. The nicotinamide−ribose moiety provides stabilizing van der Waals contacts with the closed form of the loop (specifically backbone/side chain atoms of residues 16−20) and one hydrogen bond with the nicotinamide [NADP(NN7)−I14(O)] (Figures 5A and 6A). When the nicotinamide−ribose is bound and the NADP(NN7)−I14(O) hydrogen bond is formed, a 180° rotation about ψ^{I14} is inhibited, thereby inhibiting conversion to the occluded conformation. Binding of the adenosine moiety of NADP, however, does not ensure nicotinamide−ribose binding. Rotation about the PN−O3 bond may put the nicotinamide−ribose moiety out into the surrounding medium, again allowing formation of the occluded form. Nicotinamide−ribose binding, and hence loop closure, is strongly influenced by pteridine binding and the pteridine oxidation state.

Binding of the nicotinamide−ribose moiety is stabilized by contact with the juxtapositioned pteridine ring of the substrate. In the NADPH complex, when the pteridine pocket is unoccupied, the nicotinamide−ribose binding pocket is only about 75% occupied, as judged from electron density maps in space group $P2_12_12_1^B$ (Figure 8A). For the remainder of the time, the nicotinamide−ribose is in bulk solvent, via a rotation about the PN−O3 bond of the pyrophosphate moiety. However, 75% occupancy is enough to make the closed conformation visible in electron density maps, with an average main chain temperature factor of 40 Å^2. (In the NADP$^+$ complex, the nicontinamide−ribose pocket is primarily unoccupied, rendering the loop nearly invisible with an average main chain temperature factor of 50 Å^2.) When the pteridine pocket is occupied by FOL or MTX (analogues of the Michaelis and transition complexes),

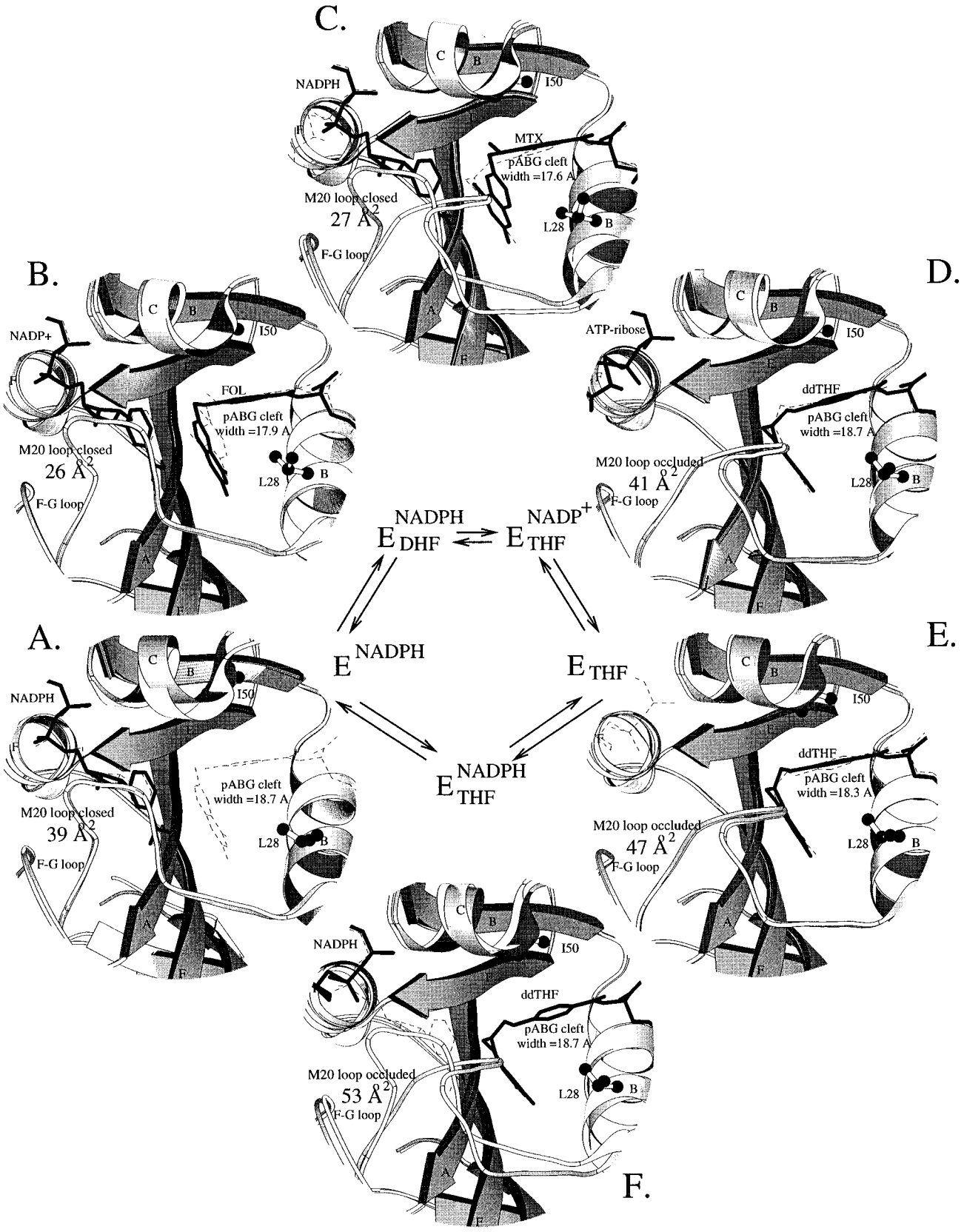

FIGURE 8: Reaction pathway analogue structures in space group $P2_12_12_1$[B]: (A) NADPH complex, (B) FOL·$NADP^+$ complex, (C) MTX·-$NADP^+$ complex, (D) ddTHF·ATP-ribose complex, (E) ddTHF complex, and (F) ddTHF·NADPH complex. In the center is drawn the kinetic pathway of the ecDHFR-catalyzed reaction as determined by Fierke et al. (1987). ecDHFR is abbreviated as E. The symbol for each intermediate appears next to the picture of its ecDHFR·analogue complex. Each structure (shaded in gray) is superposed with the sequentially subsequent analogue structure (solid white with ligands drawn in dotted lines). The average main chain temperature factor of the M20 loop and pABG cleft width are noted in each structure. This figure was produced using the graphics program Molscript (Kraulis, 1991).

van der Waals contacts between nicotinamide and pteridine rings increase the stability of nicotinamide binding, effecting 100% occupancy in the nicotinamide binding pocket and lowering the average temperature factors of the loop to 26 Å^2 in the closed loop conformation (Figure 8B,C).

Binding of the nicotinamide−ribose moiety is destabilized by steric clash with the reduced pteridine ring. Compared to FOL (in FOL·$NADP^+$), ddTHF (in ddTHF·$NADP^+$)

puckers at C6 and protrudes further into the nicotinamide binding site. Superposition of holoenzyme and ddTHF·NADP$^+$ structures reveals that, if the nicotinamide were in the binding pocket, there would be a 1.8 Å overlap between C4 of the nicotinamide and C7 of ddTHF [see Figure 5 of Reyes et al. (1995)]. The evident result of this overlap is that the nicotinamide is rotated out of the binding pocket and is disordered in solvent in the ddTHF·NADP$^+$ ternary structure ($P2_12_12_1^A$) (Figure 8D). Release of the nicotinamide moiety breaks the NADP(NN7)−I14(O) hydrogen bond and allows ψ^{I14} to rotate in transition to the occluded form, as observed in ddTHF·NADP$^+$ ($P2_12_12_1^A$) and ddTHF·ATP-ribose ($P2_12_12_1^B$). Upon NADP$^+$ release, the loop remains occluded. Without nicotinamide bound, ψ^{I14} remains free to rotate in transition to the occluded form, as inferred from the ddTHF binary complex ($P2_12_12_1^B$) (Figure 8E). Subsequent binding of NADPH also produces no difference in loop conformation from that of the preceding two complexes. In the ddTHF·NADPH complex ($P2_12_12_1^B$), nicotinamide remains unbound and the loop remains in the occluded conformation (Figure 8F).

Transition from the closed to occluded conformations necessitates that torsion angles rearrange from β-strand/hairpin to 3_{10} helix, ψ^{I14} must rotate 180°, main chain hydrogen bonds must be broken and then reformed, hydrogen bonds with the F−G loop must be broken, and hydrogen bonds with the G−H loop must be formed. This extensive rearrangement of torsion angles and hydrogen bonds proposed to occur in the interconversion between the closed and occluded conformations is neither unprecedented nor thermodynamically unreasonable. Although it is true that a large number of enzymes conserve the amount of structural rearrangement by moving a rigid flap on a pair of hinges [*e.g.* triosephosphate isomerase (Noble et al., 1993), lactate dehydrogenase (Gerstein & Chothia, 1991), and penicillopepsin (James et al., 1982)], another group of enzymes is characterized by loop motions that, like that of ecDHFR, involve extensive reorganization of backbone torsion angles [*e.g.* thymidylate synthase (Noble et al., 1990), RuBisCo (Schreuder et al., 1993), and Fab 7/19 (Schulze-Gahmen et al., 1993)]. Such reorganization may be a common, low-barrier mechanism of loop movement. With the exclusion of crystal packing interactions, the sum total of stabilizing interactions seems qualitatively equivalent in the closed and occluded conformations, a necessary requirement for rapid interconversion. The fact that crystal packing interactions, themselves normally considered weak forces, effectively compete with the ligand for conformational control of the M20 loop further suggests a low-energy barrier for the transition. Indeed, NMR studies of the ^{15}N-labeled ecDHFR·FOL complex suggest that the loop movement may be very fast (Epstein et al., 1995). Structural fluctuations on the nanosecond time scale for residues 16−19 of the M20 loop and residues 120−124 of the F−G loop are indicated.

Another mechanistic motif characteristic of active site loop movements (such as the M20 loop) is the participation of neighboring floppy loops (such as the F−G and G−H loops). The closed, open, and occluded conformations of the M20 loop are each characterized by a particular pattern of hydrogen bonds with the F−G and G−H loops. Moreover, the motion of the M20 loop depends on the freedom of movement of the F−G loop (recall that parts of the F−G loop are disordered when the M20 loop is disordered and that lattice interference with the F−G and G−H loops has been correlated with immobilization of the M20 loop in the majority of crystal forms). The active site loops of enzymes such as triosephosphate isomerase (Wierenga et al., 1992), RuBisCo (Schreuder et al., 1993), and staphylococcal nuclease A (Hodel et al., 1994) similarly display altered hydrogen-bonding patterns with neighboring flexible loops in closed and open conformations. It is intriguing that nature has designed multiple neighboring flexible loop motifs at the active site entrance of so many enzymes. Perhaps the participation of neighboring floppy loops destabilizes the end points of loop motion, preventing the loop from becoming trapped in either an open or closed position and consequently slowing diffusion of ligands to and from the active site.

Improved View of Subdomain Rotation. Subdomain composition was determined with the aid of Cα−Cα distance difference plots, as described previously in Bystroff and Kraut (1991). In addition to visual inspection, the distance difference plots were analyzed using two related algorithms, one by Nichols (Nichols et al., 1995) and the other by Fauman (Perry et al., 1990). Given a distance difference matrix, the programs search for the largest pieces of structure for which internal relative movements of α-carbons do not exceed a given threshold value (ϵ). With adjustments of ϵ, the molecule could be subdivided into rigid pieces of a meaningful size. Typically $\epsilon = 0.15-0.20$ Å for isomorphous comparisons yielded two discrete subdomains with rigid bodies of approximately 50 residues each. Subdomain composition remains stable in this range of ϵ. Comparable results were obtained with either program in isomorphous comparisons within space groups $C2$, $P2_12_12_1^B$, and $P3_221$. Results were particularly definitive when comparing holoenzyme with the MTX·NADP ternary complexes, the pair exhibiting the largest subdomain rotation. For example, in space group $P2_12_12_1^B$, this analysis yielded two rigid cores: residues 3−6, 8, 10, 12, 14, 26, 90, 103, 107−116, 118, 122, 124−127, 136−138, 140, and 146−158 in core 1 and residues 1, 2, 40−44, 46−49, 62−66, 73−84, 89, 90, 92, 93, 95, 96, 98, 99, 101−104, and 106 in core 2 (Figure 9A). Residues not counted among these cores can be assigned to a subdomain on the basis of connectivity. Subdomain 1 is best described as residues 1−37 and 107−159, while subdomain 2 is best described as residues 38−106 (Figure 9B).

This subdomain composition indicates that the rotation axis describing relative subdomain motions lies between strands A and E, and structural analysis suggests why. An interruption in hydrogen bonding between strands A and E produces a gap between them that forms the nicotinamide binding pocket (Figure 9C). Due to this interruption, there are only four hydrogen bonds between strands A and E, the fewest hydrogen bonds of any pair of strands in the enzyme (strands B and E have equally few). Moreover, the twist between strands A and E is 41°, the greatest between any pair of strands in the enzyme (average twist = 24°), increasing the freedom of motion between the subdomains. Analysis of secondary structure clustering of *L. casei* DHFR, another bacterial DHFR, supports the choice of subdomain composition (Sowdhamini & Blundell, 1995). The combination of weak hydrogen bonding, a large twist angle, and discrete structural clustering allows movement about an axis between strands A and E.

This subdomain composition is appreciably different from that assigned earlier by Bystroff and Kraut (1991), in which only nonisomorphous structures were compared. Subdomain

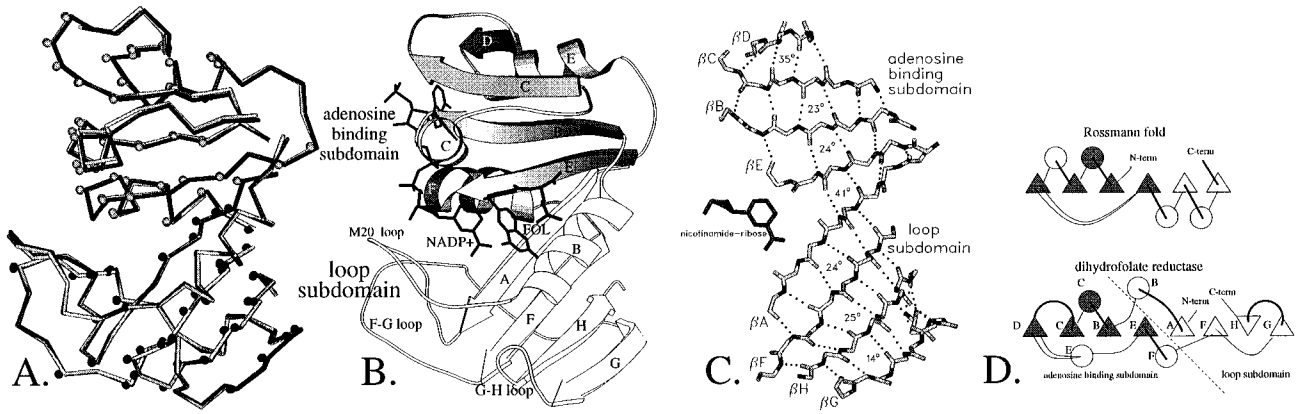

FIGURE 9: (A) Superposition of α-carbon traces of MTX·NADP$^+$ (black) and NADPH complexes (gray) in space group $P2_12_12_1{}^B$. Black dots indicate residues belonging to rigid core 1, while white dots indicate residues belonging to rigid core 2 (see text). (B) Resulting division into subdomains from rigid body analysis. (C) Backbone atoms of the central β-sheet. Twist angle between strands is noted. Hydrogen bonds are fewest and twist is the greatest (41°) between strands A and E. (D) Comparison of Rossmann fold and the ecDHFR fold. The shaded area corresponds to common features. This figure was produced using the graphics programs Setor (Evans, 1993) and Molscript (Kraulis, 1991).

1 (1−37 and 107−159) is smaller than Bystroff's major subdomain (1−37 and 89−159), and subdomain 2 (36−108) is larger than Bystroff's adenosine binding subdomain (38−88). Enlargement of subdomain 2 appends β-strand E and helix F. The adenosine binding subdomain now includes all the protein atoms involved in binding the adenosine 2′-phosphate−5′-diphosphate moiety. The new subdomain definition also corresponds to the largest portion of DHFR topologically in common with the Rossmann fold (Birktoft & Banaszak, 1984) (Figure 9D). Meanwhile, diminution of the major subdomain makes it more nearly equal in size with the adenosine binding subdomain. The diminished major subdomain is now more descriptively termed the "loop subdomain", reflecting the fact that it contains the three principal loops: the M20 loop, the F−G loop, and the G−H loop accounting for about 45% of this subdomain. The crucial difference from previous studies was the use of isomorphous (as opposed to nonisomorphous) structures in the analysis. The earlier choice of subdomains was misguided by the fact that crystal packing, as well as the ligated state, can affect relative rotation between subdomains.

Influence of Crystal Packing on Subdomain Rotation. Crystal packing clearly distorts subdomain rotation in both composition and magnitude, making isomorphous comparisons preferable for an accurate characterization. Nonisomorphous comparisons between different ligated states in space groups $C2$, $P2_1$, $P2_12_12_1{}^B$, and $P3_221$ result in deviations in subdomain composition of about 10−20 residues near the rotation axis. Furthermore, nonisomorphous comparisons between identical ligated states result in deviations in the magnitude of rotation of up to 3°. Since subdomain rotation relates two halves of the molecule, crystal packing contacts virtually anywhere on the DHFR molecule can conceivably affect subdomain rotations. As noted above, the distortion becomes significant when comparing DHFR molecules from different lattices which have been distorted in different areas of the molecule. This is especially true when determining the position of the rotation axis since, by definition, the axis is located where the least motion occurs and small lattice-induced distortions can more easily alter its position. Hence, characterization of subdomain rotation *as it would appear in solution* (in the absence of lattice interference) is most accurately derived from isomorphous comparisons, preferably from more than one series of isomorphous structures, as we have done in space groups $C2$, $P2_1$, $P2_12_12_1{}^{A,B}$, $P3_221$, and $P6_1$.

Encouragingly, the degree of subdomain rotation within a series of analogue complexes maintains the same order from crystal form to crystal form [*i.e.* among crystal forms $C2$, $P2_1$ (molecules A and B), $P2_12_12_1{}^{A,B}$, and $P3_221$]. Cleft width is used as a measure of subdomain rotation, though small independent movements of helices B and C also alter the pABG cleft width. The distance between the axis of helix C at its C terminus and the axis of helix B at its N terminus is taken as the pABG cleft width. In order of increasing pABG cleft size, MTX < ddTHF < FOL in binary complexes. When cofactor is bound, FOL and ddTHF switch order, MTX·NADP < FOL·NADP < ddTHF·NADP $\approx$ NADP. The constancy of this order among crystal packings indicates some degree of accuracy in determining the dynamics of subdomain rotation during the catalytic cycle.

Subdomain Rotation during the Catalytic Cycle. A consensus of crystallographic evidence from several series of isomorphous complex structures, as presented here, suggests that the pABG cleft opens and closes twice during the catalytic cycle (Figure 8). Specifically, the evidence suggests that the holoenzyme begins the reaction cycle with the subdomains in the open state, and then upon substrate binding, the subdomains rotate closed, and perhaps even more closed in the transition state. This scenario follows from isomorphous comparisons in space groups $C2$, $P2_12_12_1{}^B$, and $P3_221$ which indicate that the pABG cleft closes 0.7 ± 0.2 Å upon FOL (DHF analogue) binding to the holoenzyme. Similar comparisons in space groups $C2$, $P2_1$, $P2_12_12_1{}^B$, and $P3_221$ indicate that the cleft closes 0.5 ± 0.4 Å tighter when MTX replaces FOL in the ternary complex, possibly reflecting subdomain behavior in the transition state. Further evidence suggests that, upon hydride transfer, the subdomains rotate open and then close again after NADP$^+$ release. Isomorphous comparisons in space group $P2_12_12_1{}^B$ indicate that the pABG cleft opens to its widest extent in the ddTHF·ATP-ribose/NADP$^+$ complexes and then shrinks 0.5 Å upon release of cofactor. Finally, it appears that rebinding of NADPH causes the subdomains to rotate open, completing the cycle. The structure of ddTHF·NADPH in space group $P2_12_12_1{}^B$ shows that the cleft has returned to the open state as in the ddTHF·ATP-ribose/NADP$^+$ complex. The influ-

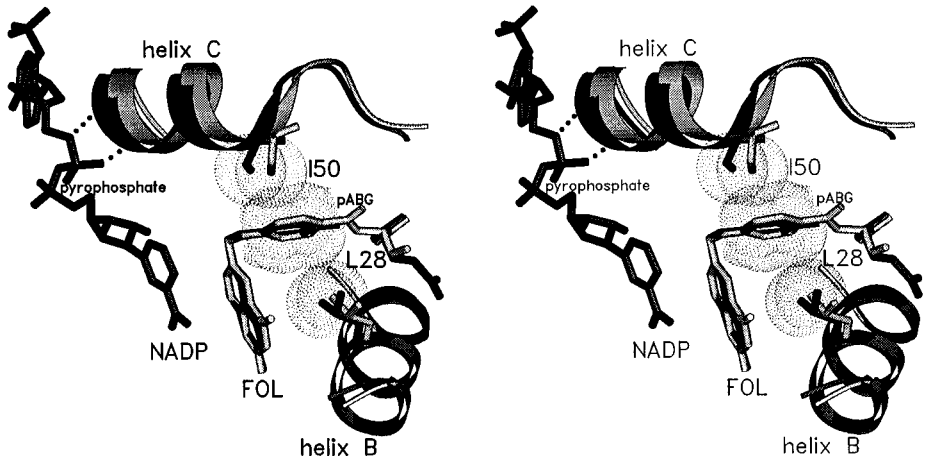

FIGURE 10: Superposition of FOL and FOL·NADP$^+$ complexes in space group $P2_12_12_1^B$. Interaction with the pyrophosphate moiety produces a 0.7 Å shift of helix C upon cofactor binding. The shift allows hydrogen bonding between pyrophosphate oxygens and the N-terminal amide nitrogens of the helix. The shift also brings I50 of the pABG cleft 0.7 Å closer to the nicotinamide. This shift may stabilize the pteridine's close contact with nicotinamide via I50's interaction with the pABA ring. This figure was produced using the graphics program Setor (Evans, 1993).

ence of crystal packing on subdomain rotation hints that the range of subdomain motion may be dampened within a series of isomorphous structures and that subdomain rotation in solution may be larger than observed within any particular crystal form.

Mechanism of Subdomain Rotation. Isomorphous comparisons of holoenzyme and ternary complex structures in space groups $C2$, $P2_12_12_1^B$, and $P3_221$ suggest that subdomain rotation is induced by the pABG moiety. Subdomain rotation produces its largest relative movement between helix B of the loop subdomain and helix C of the adenosine binding subdomain, the two walls of the pABG binding cleft. The side chains of L28 from helix B and I50 from helix C are attracted 0.7 ± 0.2 Å closer together by van der Waals forces with the sandwiched pABG moiety (Figure 8A,B). The motion imparted on helices B and C appears to be spread over both subdomains by a shear mechanism (Gerstein et al., 1994). Helices B and C shear with respect to the sheet, and to a lesser extent, the individual strands shear with respect to their neighbors, producing the motion described as a rotation between the two subdomains. It appears that the rotation can be produced by multiple combinations of very slight side chain movements (between 0.1 and 0.2 Å), giving the position of the intersubdomain axis a great deal of play [as noted in Bystroff and Kraut (1991)] and making it vulnerable to distortions imparted by crystal contacts.

On the basis of isomorphous comparisons between FOL·NADP$^+$ and MTX·NADP complexes in space groups $C2$, $P2_1$, $P2_12_12_1^B$, and $P3_221$, MTX can produce a more closed subdomain rotation than FOL, closing the pABG cleft another 0.5 ± 0.4 Å (Figure 8C). Cleft shrinkage may be due to an altered position of the pABG moiety as compared to that of FOL. The pABG of MTX is shifted 1.0 Å along the pABG cleft relative to that of FOL (Reyes et al., 1995). As will be argued, enhanced interactions with the shifted pABG moiety allowed by a larger subdomain rotation may stabilize puckering of the pteridine's C6 in the transition state.

A more open subdomain rotation is produced in ternary product analogue complex ddTHF·NADP$^+$ due to a shift in helix B's position (Figure 8C). Reduction of the dihydropteridine ring produces a pucker at C6, and the pABG moiety shifts 0.8 Å along the pABG binding cleft, much as in the case of MTX, as described in Reyes et al. (1995). By analogy with MTX, we would expect a more closed subdomain rotation. Indeed, ddTHF favors a more closed subdomain rotation than FOL in binary complexes in space groups $P2_12_12_1^B$ and $P6_1$. However, in the ternary complex ddTHF·ATP-ribose, helix B translates 0.5 Å in response to a shift in M20 loop conformational equilibrium from closed in the transition state analogue (MTX·NADPH) to occluded (Figure 8D). The translation places helix B closer to the G−H loop so that the M20 loop and G−H loop may form a pair of hydrogen bonds [N23(O)−S148(N) and N23(N)−S148(Oγ)], as is characteristic of the occluded conformation. Translation of helix B also alters L28−pABG interactions such that they no longer are in van der Waals contact. In the absence of this van der Waals contact, subdomain rotation favors the open state. The combination of helix translation and subdomain rotation widens the pABG binding cleft to its maximal size, 1.1 Å wider than in the transition state analogue (MTX·NADPH in space group $P2_12_12_1^B$).

The ability of the subdomains to rotate closed is restored upon NADP$^+$ release. NADP$^+$ release produces a translation along the helical axis of helix C, 0.7 Å toward the pABG cleft and away from the pyrophosphate of NADP. Apparently, loss of pyrophosphate hydrogen bonds with the N terminus of helix C releases the helix to move toward the pABG moiety (Figures 8E and 10). The translation compensates for the aforementioned helix B movement by closing the cleft between I50 and L28, improving contact with the pABG moiety. With van der Waals contact restored between L28 and the pABG moiety, domain rotation is able to close, though not as far as in the FOL·NADP$^+$ ternary complex. Upon binding of NADPH, the pyrophosphate draws helix C 0.7 Å away from the pABG once more, favoring an open subdomain rotation (Figure 8F).

Structural Rigidity of Vertebrate DHFRs. In contrast to ecDHFR, vertebrate DHFRs appear to be more rigid. Comparison of crystal structures offers no hint of loop I motion (loop I is the equivalent of the M20 loop of ecDHFR) or subdomain rotation. Loop conformations of chicken (Matthews et al., 1985a,b; McTigue et al., 1992, 1993), mouse (Stammers et al., 1987), and human (Oefner et al., 1988; Davies et al., 1990) DHFRs are invariably closed regardless of species, crystal packing, or ligated state. Subdomain rotation is also unobserved in isomorphous or

nonisomorphous comparisons. Curiously, DHFRs from both *E. coli* and vertebrate sources perform the same catalytic function, exhibit similar kinetic pathways, and share a similar architecture, but one is conformationally flexible and the other rigid. This unique system puts us in a position to suggest which structural features are responsible for endowing flexibility in ecDHFR and, more enlightening, what the role of flexibility in general may be.

Three structural differences between ecDHFR and vertebrate DHFR may account for the difference in flexibility of their loops. (1) Truncation of the vertebrate's G−H loop prevents formation of hydrogen bonds with loop I, an apparently necessary prerequisite for forming the occluded or open conformations found in ecDHFR. (2) Insertion of a left-handed polyproline-type helix in vertebrate DHFR's loop I (accompanying the insertion of P25) increases the rigidity of the loop, a feature not present in ecDHFR's M20 loop. (3) In keeping with the observed requirement of glycine or proline in position 3 of a type III′ hairpin, vertebrate DHFR places G20 in this position of loop I's central hairpin. The favorable placement of this glycine stabilizes hairpin formation and hence the closed conformation. *E. coli*'s equivalent, N18, also in position 3 of the type III′ central hairpin, is not as energetically favorable in position 3 and thus facilitates rearrangement to other conformations.

Less obvious is the structural basis for increased rigidity between subdomains in vertebrate DHFRs. In vertebrate DHFR and ecDHFR, there is the same small number of hydrogen bonds between strands A and E, the intersubdomain border. Vertebrate DHFR also maintains the same large twist angle between strands A and E, 41°. Moreover, packing analysis of human DHFR has identified the same two subdomains found in ecDHFR (Siddiqui & Barton, 1995). Hence, we can offer no convincing structural explanation for why subdomain rotation has not been crystallographically observed in vertebrate DHFRs.

Role of Flexibility in Substrate Binding. M20 loop and subdomain movements achieve their most open conformation in the absence of nicotinamide and pABG binding, suggesting that improved active site accessibility may be involved in the substrate binding process. The open M20 loop conformation, a likely component of loop motion in the absence of nicotinamide binding, produces an 8 Å opening to the active site, more than wide enough to pass a nicotinamide ring from the solvent to the binding pocket (Figure 6B). Similarly, the open subdomain rotation produces a 0.7 Å wider pABG binding cleft in the holoenzyme (as compared to the FOL·$NADP^+$ complex), presumably facilitating binding of DHF (Figure 8A). The requirements of substrate access have long been proposed as a reason for the widespread observation of open loop and open domain conformations (Wolfenden, 1974). Indeed, theoretical calculations also suggest that structural fluctuations such as these can lead to lowering of free energy barriers to the binding process (Karplus & McCammon, 1983).

Observation of a similar range of variation in pABG cleft size in vertebrate DHFRs supports the hypothesis that motion is important in the substrate binding process. However, instead of subdomain rotation, the width of the pABG cleft in vertebrate DHFRs is regulated by movements of a loop connecting helix C and strand C (residues 59−70). The pABG cleft is 0.8 Å wider when pABG is not bound, as observed in comparisons between chicken DHFR·biopterin·-$NADP^+$ and human DHFR·FOL (McTigue et al., 1992). Although DHFRs from *E. coli* and vertebrate sources employ different mechanisms, the effect is the same, to open the cleft for DHF binding. The fact that evolution devised two different mechanisms for introducing flexibility in pABG cleft width suggests that this type of motion is important to DHFR catalysis. The vertebrate mechanism may be more efficient, as DHF binding rates are 4−5 times faster for human than for *E. coli* (Appleman et al., 1990; Fierke et al., 1987).

Since an open conformation of loop I is not conserved in vertebrate DHFRs, evidently, the exaggerated loop motion of the M20 loop of ecDHFR is not essential for cofactor binding in vertebrate DHFRs; cofactor binding rates are similar for vertebrate and bacterial DHFRs. The nicotinamide moiety may gain access to the vertebrate binding pocket with smaller scale loop fluctuations. Interestingly, it is possible that the exaggerated loop motion in ecDHFR is an evolutionary adaptation to the particular environment of the prokaryotic cell, as will be argued later.

Role of Flexibility in Proton Transfer. Some evidence suggests that M20 loop flexibility facilitates protonation at N5 of DHF by admitting a proton-donating water molecule to the active site. Protonation of N5, a likely prerequisite for hydride transfer, has been observed by Raman spectroscopy in ecDHFR·DHF·$NADP^+$ and thus presumably also occurs in the Michaelis complex (Chen et al., 1994). However, the mechanism of protonation is poorly understood, particularly since no proton-donating group within hydrogen-bonding distance of N5 has been observed in Michaelis analogue complexes. When the M20 loop is in the closed conformation, the side chain of M20 effectively excludes water molecules from the vicinity of N5. But a water molecule is found hydrogen bonding to O4 (2.8 Å) and close to N5 (3.2 Å) when the loop is open, and the M20 side chain has moved [ecDHFR·FOL·$NADP^+$ (space group *C*2) and in ecDHFR·FOL (space group $P6_1$) (Reyes et al., 1995)]. If the open conformation of the M20 loop is indeed an intermediate between closed and occluded forms as proposed earlier, then a water molecule would have intermittent access to N5 as seen in the *C*2 space group. Such a movement may account for an observed obligatory isomerization in the ternary substrate ecDHFR or *La. casei* DHFR complex preceding hydride transfer (Beard et al., 1989). Similarly, rotation of Y/F31 in vertebrate DHFRs has been implicated in performing the role of gate for the proton-donating water molecule (McTigue et al., 1992). Following protonation, return to the closed loop conformation would place M20 back into position to exclude water from the active site, a feature that presumably facilitates hydride transfer in several other dehydrogenases/reductases (Eklund & Brändén, 1987).

Role of Flexibility in Transition State Stabilization. Two salient features of the transition state for hydride transfer are a sub van der Waals contact between hydride donor and acceptor and puckering of C6 of the pteridine ring. As a catalyst, DHFR must stabilize these transition state features. Prior structural work suggests that, although MTX, the tight-binding inhibitor of DHFR, does not itself represent the transition state, its unique binding geometry in the MTX·-NADPH complex allows the enzyme molecule to adopt a conformation that appears to (1) stabilize sub van der Waals contact between hydride donor and acceptor and (2) stabilize

puckering of C6 of the pteridine ring (Bystroff & Kraut, 1991). These ideas are supported and modified in light of new evidence.

The calculated optimal geometry for the transition state for hydride transfer places the hydride donor (C4) and acceptor (C6) within 2.6 Å of each other (Wu & Houk, 1987), a distance 1 Å shorter than the sum of their van der Waals radii. It has been well documented by Bystroff et al. (1990), Brown and Kraut (1992), and Reyes et al. (1995) that just such an overlap between the nicotinamide and pteridine binding pockets is a feature of the DHFR structure. Their evidence includes studies in which binary folate and holoenzyme structures are superposed, revealing what would be a 2.8 Å contact between the hydride donor and acceptor. Furthermore, in FOL·$NADP^+$ complexes (space groups *C*2, $P2_12_12_1^B$, and $P3_221$), sub van der Waals contacts between the nicotinamide and the FOL pteridine ring (between 3.2 and 3.3 Å) are apparent. But in the MTX·NADPH complex, the nicotinamide is able to penetrate the pteridine binding pocket further than it can when FOL is present since MTX's pteridine is flipped 180° with respect to that of FOL. This flip (approximately about the C6−C9 bond) creates a vacancy where C6 of FOL normally resides (Bystroff & Kraut, 1991). If the isomorphous $P2_12_12_1^B$ structures, MTX·NADPH and FOL·$NADP^+$, are superposed, C4 from the nicotinamide of MTX·NADPH is only 2.9 Å from C6 of FOL, very close to the theoretical 2.6 Å distance calculated for the transition state of hydride transfer (Figure 8B). Thus, the position of the nicotinamide in the MTX·NADPH complex may in fact reflect transition state geometry as originally hypothesized by Bystroff and Kraut (1991). Further stabilizing close contact between the nicotinamide and pteridine ring of MTX is the closed M20 loop conformation. The additional hydrogen bond [NADP(NN7)−I14(O)] and van der Waals contacts with the nicontinamide−ribose provided by the closed form of the M20 loop stabilize the juxtapositioned ligands. A large decrease in the hydride transfer rate upon deletion of the central portion of the M20 loop supports this hypothesis (Li et al., 1992).

Pursuing another aspect of the transition state, transfer of the hydride ion is expected to be facilitated by puckering of C6 of the pteridine ring. A consequence of the pucker is likely to be a shift of the pABG moiety in the direction observed in the product analogue complex with ddTHF, though probably not as far. In the ddTHF complex, the pABG moiety is shifted 0.8 Å along the length of the pABG crevice away from its position in FOL. Reyes et al. (1995) noted that the pABA ring of FOL is situated closer to I50 than to L28, implying a strained binding geometry, but in ddTHF, the pABA ring is nearly equidistant from L28 and I50. This observation was taken as evidence that ecDHFR is designed to bind the pABA ring in a shifted position, as in ddTHF, a position that should stabilize puckering at C6 in the transition state. Another manifestation of the favored binding of the extended pABG position may be the more closed subdomain rotation observed in ddTHF binary complexes (but not ternary complexes) and MTX binary and ternary complexes. Due to its flipped-over pteridine, the pABG of MTX also binds in a shifted position, analogous to that of ddTHF and presumably the transition state. Particularly in MTX ternary complexes, it has been shown that MTX binds to ecDHFR, producing a subdomain rotation that closes the pABG cleft 0.5 ± 0.4 Å further than FOL. If the closed pABG cleft is indicative of enhanced hydrophobic interactions between the enzyme and the shifted pABA ring, then the closed subdomain rotation may also play a role in stabilizing puckering at C6 in the transition state of hydride transfer. The idea that subdomain rotation stabilizes puckering at C6 is related to that of Bystroff and Kraut (1991) (see especially Figure 8 therein), though the pABA movement produced by puckering at C6 is now known to be different from that predicted in 1991.

One other means of transition state stabilization, separate from our considerations of MTX, is suggested from comparing the FOL binary complex with the ternary complex. Close approach of reactants in the transition state for hydride transfer may be further stabilized by conformational shifts of helix C upon cofactor binding. In $P2_12_12_1^B$, $NADP^+$ binding to the FOL binary complex accompanies a 0.7 Å translation of helix C along its helical axis, bringing its N-terminal backbone amide nitrogens within hydrogen-bonding distance of the pyrophosphate oxygens (Figure 10). Consequently, the C terminus of helix C, bearing I50 of the pABG cleft, is also shifted 0.7 Å toward the pyrophosphate. However, if the pABG moiety were to remain in contact with I50, the pteridine would also be translated 0.7 Å toward the nicotinamide ring, but such a translation is impeded by steric clash between the pteridine and nicotinamide rings. The molecular "tug of war" over helix C may indicate another strategy the enzyme employs to stabilize the close proximity of nicotinamide and pteridine rings, a way of using both the cofactor's pyrophosphate moiety and dihydrofolate's pABG moiety as handles to stabilize the transition state.

Role of Flexibility in Product Release. Helix C movement also may play a role in regulating THF release from the binary complex. Following hydride transfer and $NADP^+$ release, the N terminus of helix C is freed from hydrogen bonding with the pyrophosphate moiety of $NADP^+$, allowing helix C to shift 0.7 Å back toward the pABG moiety. Consequently, I50 returns to its position in van der Waals contact with the pABG moiety. The closer interaction presumably tightens the enzyme's grip on ddTHF. Tightening THF binding in the binary complex may prevent formation of the apoenzyme. An increased concentration of apoenzyme would lead to an increased percentage of inactive enzyme, as the apoenzyme exists in a 50/50 equilibrium between active and inactive forms (Cayley et al., 1981; Fierke et al., 1987).

NADPH-assisted release of THF is a distinctive characteristic of the DHFR-catalyzed reaction (Fierke et al., 1987). The off rate for THF is 6-fold higher from the ternary complex than from the binary complex (Fierke et al., 1987). Upon rebinding a second molecule of NADPH, helix C translates away from the pABG moiety again, widening the cleft to its maximum width and probably assisting THF release. Widening of the pABG cleft via helix C may be partly responsible for the observed elevation in THF off rate upon rebinding of NADPH. Perturbation of the finely adjusted balance of conformational shifts of helix C is likely responsible for the behavior of helix C mutants. A triple mutation in helix C (H45R, W47Y, and I50F) diminishes the NADPH-assisted THF off rate (Li & Benkovic, 1991), while the R44L mutation enhances the NADPH-assisted THF off rate (Adams et al., 1989).

It may be expected that NADPH-assisted release of THF via helix C would be equally achieved by $NADP^+$ since pyrophosphate, the moiety inducing the helix shift, is common to both NADPH and $NADP^+$. Indeed, there is a

negative cooperativity in THF binding to the ternary product complex; the K_d of THF is nearly 2-fold higher in the THF·NADP$^+$ ternary complex than in the binary complex. However, the effect is much weaker than the 6-fold effect measured in the THF·NADPH complex. The difference between the oxidized and reduced cofactor's ability to assist THF release may be due to differences in nicotinamide binding affinity. The reduced nicotinamide has a greater tendency to occupy the nicotinamide binding pocket as shown in NADPH *vs* NADP$^+$ isomorphous complexes ($P2_12_12_1^B$). NMR studies on NADPH *vs* NADP$^+$ binding to ecDHFR are in agreement with this finding (Cayley et al., 1980). Theoretical calculations suggest that this difference may be due to the enzyme's complementarity to the nicotinamide−ribose torsion angle preferred by NADPH as opposed to NADP$^+$ (Wu & Houk, 1991). Since the binding pockets for the nicotinamide of NADPH and the pteridine of ddTHF overlap by nearly 2 Å [as determined by superpositioning studies (Reyes et al., 1995)], the reduced nicotinamide's higher binding affinity would more effectively compete for binding and hence offer greater assistance to THF off. Furthermore, the size of the helix C shift is dependent on nicotinamide binding; the pyrophosphate moiety produces a greater helix C shift when nicotinamide is bound than when it is unbound (as shown in comparisons of FOL·NADP$^+$ and FOL·ATP-ribose). Proper binding of nicotinamide, in turn, would strengthen pyrophosphate binding, producing a larger helix C shift which would presumably assist THF release.

Role of Flexibility in Product Inhibition. The relative binding affinity for NADP$^+$ *vs* NADPH [K_d (NADP$^+$)/K_d (NADPH)] is 2 times greater for ecDHFR than for human DHFR. Moreover, K_d (NADP$^+$)/K_d (NADPH) in the DHF ternary complex is 100 times greater for ecDHFR than for human DHFR (Fierke et al., 1987; Appleman et al., 1990). As proposed by Appleman et al. (1990), this trend may reflect an evolutionary adaptation to cellular differences in NADP$^+$/NADPH concentrations. In eukaryotic cells, NADP$^+$ concentrations are no more than 1% of NADPH concentrations, whereas in prokaryotic cells, NADP$^+$ concentrations are comparable to NADPH concentrations. To prevent product inhibition under conditions of higher product concentrations, ecDHFR appears to have evolved to decrease its affinity for product (NADP$^+$). M20 loop flexibility may be responsible for the difference in product affinity.

A salient feature of the mechanism of ecDHFR's M20 loop movement is a 180° flip of ψ^{I14} required to convert between closed and occluded conformations. Rotation of this peptide toward its position in the occluded conformation removes one of three hydrogen bonds with the carboxamide nitrogen (NN7) of NADP. The oxidized form of NADP is particularly sensitive to disruption of this hydrogen bond as its carboxamide group rotates freely, while that of NADPH is constrained in the plane of the nicotinamide ring by conjugation. Overall, the effect of introducing loop motion should preferentially increase the entropy cost of binding oxidized nicotinamide over reduced nicotinamide. The oxidized nicotinamide's diminished ability to form this hydrogen bond is shown by a 10 Å^2 difference in the temperature factor between M20 loop main chain atoms in ecDHFR·NADP$^+$ (40 Å^2) and ecDHFR·NADPH (50 Å^2) (space group $P2_12_12_1^B$). For I14(O) in particular, there is a 28 Å^2 difference in the temperature factor between ecDHFR·NADP$^+$ (45 Å^2) and ecDHFR·NADPH (17 Å^2).

DHFR Movie. A movie portraying inferred loop and subdomain movements as a function of the reaction coordinate was constructed on the basis of crystallographic results reported here. The hypothetical sequence of events is the same as reported for ecDHFR under cellular conditions (Figure 8); however, no effort was made to scale the timing of events to the measured pre-steady state rates (Fierke et al., 1987). Likewise, no effort was made to simulate Newtonian dynamics of the transitions. The main purpose of the movie is to illustrate the range of loop and subdomain movements and the sequence of their occurrence along the reaction coordinate.

The movie is based on several ecDHFR complex structures in $P2_12_12_1^B$. The holoenzyme, FOL·NADP$^+$, MTX·NADPH, ddTHF·ATP-ribose, ddTHF, and ddTHF·NADPH complexes are depicted in frames 1, 23, 24, 44, 51, and 56 of a 72-frame movie. Although the open loop conformation is not observed in these structures, it is proposed to be a transient intermediate in loop motion between closed and occluded conformations. It is also proposed to play a role in protonation of N5 of DHF. It is therefore included in the DHFR movie to demonstrate how the loop may interconvert between closed and occluded extremes. To smooth out the loop and domain motions, intervening frames were generated using InsightII and Discover (MSI, San Diego, CA). Energy terms were applied to force a starting conformation into the conformation of a crystal structure of a subsequent time point analogue (template-forcing constraint) via a low-energy pathway. The calculation was stopped at various time points to generate coordinates of the intermediates. No definitive information is available regarding the lifetime of loop and subdomain movements; hence, the frequency of their motion with respect to the reaction coordinate was arbitrarily chosen to minimize the number of distinct movements per cycle yet show all the movements observed. The movie was constructed with GIFMerge. The movie is available as Supporting Information. Alternatively, the movie may be viewed with the Netscape web browser at http://www-chem.ucsd.edu/Faculty/Kraut/dhfr.html.

ACKNOWLEDGMENT

We thank the personnel of the N. H. Xuong Laboratory, especially C. Nielsen, N. Nguyen, P. Datte, and D. Sullivan for aid in data collection and use of their data collection facility. We thank J. Grimsley and K. Brown for assistance in starting this project and G. Kleiger for insightful discussions. We thank S. Everse for technical assistance. We are indebted to W. Nichols for guidance in analyzing structural movements. We acknowledge the San Diego Supercomputer Center for a grant of computing time.

SUPPORTING INFORMATION AVAILABLE

Movie depicting the loop and domain motions of DHFR. This information is available only via the Internet. Ordering information is given on any current masthead page.

REFERENCES

Adams, J., Johnson, K., Matthews, R., & Benkovic, S. J. (1989) *Biochemistry 28*, 6611−6618.

Appleman, J. R., Beard, W. A., Delcamp, T. J., Prendergast, N. J., Freisheim, J. H., & Blakley, R. L. (1990) *J. Biol. Chem. 265*, 2740−2748.

Beard, W. A., Appleman, J. R., Delcamp, T. J., Freisheim, J. H., & Blakley, R. L. (1989) *J. Biol. Chem. 264*, 9391−9399.

Birktoft, J. J., & Banaszak, L. J. (1984) in *Peptide and Protein Reviews* (Hearn, M. T. W., Ed.) pp 1−46, Marcel Dekker, Inc., New York.
Blakley, R. L. (1969) in *The Biochemistry of Folic Acid and Related Pteridines* (Neuberger, A., & Tatum, E. L., Eds.) pp 219−358, North-Holland Publishing Co., Amsterdam.
Bolin, J. T., Filman, D. J., Matthews, D. A., Hamlin, R. C., & Kraut, J. (1982) *J. Biol. Chem. 257*, 13650−13662.
Brown, K. A., & Kraut, J. (1992) *Faraday Discuss. 93*, 217−224.
Bystroff, C., & Kraut, J. (1991) *Biochemistry 30*, 2227−2239.
Bystroff, C., Oatley, S. J., & Kraut, J. (1990) *Biochemistry 29*, 3263−3277.
Cayley, P. J., Feeney, J., & Kimber, B. J. (1980) *Int. J. Biol. Macromol. 2*, 251−255.
Cayley, P. J., Dunn, S. M. J., & King, R. W. (1981) *Biochemistry 20*, 874−879.
Champness, J. N., Achari, A., Ballantine, S. P., Bryant, P. K., Delves, C. J., & Stammers, D. K. (1994) *Structure 2*, 915−924.
Chen, Y.-Q., Kraut, J., Blakley, R. L., & Callender, R. (1994) *Biochemistry 33*, 7021−7026.
Cody, V., Wojtczak, A., Kalman, T. I., Freisheim, J. H., & Blakley, R. L. (1993) in *Chemistry and Biology of Pteridines and Folates* (Ayling, J. E., Nair, M. G., & Baugh, C. M., Eds.) pp 481−486, Plenum Press, New York.
Davies, J. F., Delcamp, T. J., Prendergast, N. J., Ashford, V. A., Freisheim, J. H., & Kraut, J. (1990) *Biochemistry 29*, 9467−9479.
Dion, A., Linn, C. E., Bradrick, T. D., Georghiou, S., & Howell, E. E. (1993) *Biochemistry 32*, 3479−3487.
Eklund, H., & Brändén, C.-I. (1987) in *Pyridine Nucleotide Coenzymes, Vol. 2, Part A* (Dolphin, D., Avramovic, O., & Poulson, R., Eds.) pp 51−99, Wiley, New York.
Epstein, D. M., Benkovic, S. J., & Wright, P. E. (1995) *Biochemistry 34*, 11037−11048.
Evans, S. V. (1993) *J. Mol. Graphics 11*, 134−138.
Falzone, C. J., Wright, P. E., & Benkovic, S. J. (1994) *Biochemistry 33*, 439−442.
Fierke, C. A., Johnson, K. A., & Benkovic, S. J. (1987) *Biochemistry 26*, 4085−4092.
Filman, D. J., Bolin, J. T., Matthews, D. A., & Kraut, J. (1982) *J. Biol. Chem. 257*, 13663−13672.
Fitzgerald, P. M. D. (1988) *J. Appl. Crystallogr. 21*, 273.
Gerstein, M., & Chothia, C. (1991) *J. Mol. Biol. 220*, 133−149.
Gerstein, M., Lesk, A. M., & Chothia, C. (1994) *Biochemistry 33*, 6739−6749.
Hamlin, R. (1985) *Methods Enzymol. 114*, 416−452.
Hodel, A., Kautz, R. A., Adelman, D. M., & Fox, R. O. (1994) *Protein Sci. 3*, 549−556.
Hoeltzli, S. D., & Frieden, C. (1994) *Biochemistry 33*, 5502−5509.
Howard, A. J., Nielsen, C., & Xuong, N.-H. (1985) *Methods Enzymol. 114*, 452−472.
Howell, E. E., Booth, C., Farnum, M., Kraut, J., & Warren, M. S. (1990) *Biochemistry 29*, 8561−8569.
Huennekens, F. M. (1994) *Adv. Enzyme Regul. 34*, 397−419.
Huennekens, F. M. (1996) *Protein Sci. 5*, 1201−1208.
Iwakura, M., & Tanaka, T. (1992) *J. Biochem. 111*, 31−36.
James, M. N. G., Sielecki, A., Salituro, F., Rich, D. H., & Hofmann, T. (1982) *Proc. Natl. Acad. Sci. U.S.A. 79*, 6137−6141.
Karplus, M., & McCammon, J. A. (1983) *Annu. Rev. Biochem. 53*, 263−300.
Kempner, E. (1993) *FEBS Lett. 326*, 4−10.
Knighton, D. R., Kan, C.-C., Howland, E., Janson, C. A., Hostomska, Z., Welsh, K. M., & Matthews, D. A. (1994) *Nat. Struct. Biol. 1*, 186−194.
Kraulis, P. J. (1991) *J. Appl. Crystallogr. 24*, 946−950.
Lee, H., Reyes, V. M., & Kraut, J. (1996) *Biochemistry 35*, 7012−7020.
Li, L., & Benkovic, S. J. (1991) *Biochemistry 30*, 1470−1478.
Li, L., Falzone, C. J., Wright, P. E., & Benkovic, S. J. (1992) *Biochemistry 31*, 7826−7833.
Margosiak, S. A., Appleman, J. R., Santi, D. V., & Blakley, R. L. (1993) *Arch. Biochem. Biophys. 305*, 499−508.
Matthews, D. A., Alden, R. A., Bolin, J. T., Freer, S. T., Hamlin, R., Xuong, N., Kraut, J., Poe, M., Williams, M., & Hoogsteen, K. (1977) *Science 197*, 452−455.
Matthews, D. A., Alden, R. A., Bolin, J. T., Filman, D. J., Freer, S. T., Hamlin, R., Hol, W. G. J., Kisliuk, R. L., Pastore, E. J., Plante, L. T., Xuong, N., & Kraut, J. (1978) *J. Biol. Chem. 253*, 6946−6954.
Matthews, D. A., Bolin, J. T., Burridge, J. M., Filman, D. J., Volz, K. W., Kaufman, B. T., Beddell, C. R., Champness, J. N., Stammers, D. K., & Kraut, J. (1985a) *J. Biol. Chem. 260*, 381−391.
Matthews, D. A., Bolin, J. T., Burridge, J. M., Filman, D. J., Volz, K. W., & Kraut, J. (1985b) *J. Biol. Chem. 260*, 392−399.
Matthews, D. A., Appelt, K., Oatley, S. J., & Xuong, N. H. (1990) *J. Mol. Biol. 214*, 923−936.
McTigue, M. A., Davies, J. F., Kaufman, B. T., & Kraut, J. (1992) *Biochemistry 31*, 7264−7273.
McTigue, M. A., Davies, J. F., Kaufman, B. T., & Kraut, J. (1993) *Biochemistry 32*, 6855−6862.
Morgan, W. D., Birdsall, B., Polshakov, V. I., Sali, D., Kompis, I., & Feeney, J. (1995) *Biochemistry 34*, 11690−11702.
Nichols, W. L., Rose, G. D., Ten Eyck, L. F., & Zimm, B. H. (1995) *Proteins 23*, 38−48.
Noble, M. E. M., Zeelen, J. P., & Wierenga, R. K. (1993) *Proteins 16*, 311−326.
Oefner, C., D'arcy, A., & Winkler, F. K. (1988) *Eur. J. Biochem. 174*, 377−385.
Oppenheimer, N. J. (1982) in *The Pyridine Nucleotide Coenzymes* (Everse, J., Anderson, B., & You, K.-S., Eds.) pp 51−89, Academic Press, New York.
Perry, K. M., Fauman, E. B., Finer-Moore, J. S., Montfort, W. R., Maley, G. F., Maley, F., & Stroud, R. M. (1990) *Proteins 8*, 315−333.
Reyes, V. M., Sawaya, M. R., Brown, K. A., & Kraut, J. (1995) *Biochemistry 34*, 2710−2723.
Roth, B., & Stammers, D. K. (1992) in *The Design of Drugs to Macromolecular Targets* (Beddell, C. R., Ed.) pp 85−118, John Wiley & Sons Ltd., New York.
Sawaya, M. R. (1994) Ph.D. Thesis, University of California−San Diego, La Jolla, CA.
Schreuder, H. A., Knight, S., Curmi, P. M. G., Andersson, I., Cascio, D., Brändén, C.-I., & Eisenberg, D. (1993) *Proc. Natl. Acad. Sci. U.S.A. 90*, 9968−9972.
Schulze-Gahmen, U., Rini, J. M., & Wilson, I. A. (1993) *J. Mol. Biol. 234*, 1098−1118.
Siddiqui, A. S., & Barton, G. J. (1995) *Protein Sci. 4*, 872−884.
Sowdhamini, R., & Blundell, T. L. (1995) *Protein Sci. 4*, 506−520.
Stammers, D. K., Champness, J. N., Beddell, C. R., Dann, J. G., Eliopoulos, E., Geddes, A. J., Ogg, D., & North, A. C. T. (1987) *FEBS Lett. 218*, 178−184.
Stoddard, B. L. (1996) *Pharmacol. Ther. 70*, 215−256.
Taira, K., Chen, J.-T., Mayer, R. J., & Benkovic, S. J. (1987) *Bull. Chem. Soc. Jpn. 60*, 3017−3024.
Thillet, J., Adams, J. A., & Benkovic, S. J. (1990) *Biochemistry 29*, 5195−5202.
Tronrud, D. E., Ten Eyck, L. F., & Matthews, B. W. (1987) *Acta Crystallogr. A43*, 489.
Volz, K. W., Matthews, D. A., Alden, R. A., Freer, S. T., Hansch, C., Kaufman, B. T., & Kraut, J. (1982) *J. Biol. Chem. 257*, 2528−2536.
Wierenga, R. K., Borchert, T. V., & Noble, M. E. M. (1992) *FEBS Lett. 307*, 34−39.
Wolfenden, R. (1974) *Mol. Cell. Biochem. 3*, 207−211.
Wu, Y.-D., & Houk, K. N. (1987) *J. Am. Chem. Soc. 109*, 2226−2227.
Wu, Y.-D., & Houk, K. N. (1991) *J. Am. Chem. Soc. 113*, 2353−2358.

BI962337C